

1 **Kerb and urban increment of highly time-resolved**
2 **trace elements in PM₁₀, PM_{2.5} and PM_{1.0} winter aerosol**
3 **in London during ClearfLo 2012**

4

5 **S. Visser¹, J.G. Slowik¹, M. Furger¹, P. Zotter¹, N. Bukowiecki¹, R. Dressler², U.**
6 **Flechsig³, K. Appel^{4*}, D.C. Green⁵, A.H. Tremper⁵, D.E. Young⁶, P.I. Williams^{6,7},**
7 **J.D. Allan^{6,7}, S.C. Herndon⁸, L.R. Williams⁸, C. Mohr⁹, L. Xu¹⁰, N.L. Ng^{10,11}, A.**
8 **Detournay¹², J.F. Barlow¹³, C.H. Halios¹³, Z.L. Fleming^{7,14}, U. Baltensperger¹ and**
9 **A.S.H. Prévôt¹**

10 [1] {Laboratory of Atmospheric Chemistry, Paul Scherrer Institute, Villigen,
11 Switzerland}

12 [2] {Laboratory of Radiochemistry and Environmental Chemistry, Paul Scherrer
13 Institute, Villigen, Switzerland}

14 [3] {Swiss Light Source, Paul Scherrer Institute, Villigen, Switzerland}

15 [4] {HASYLAB, DESY Photon Science, Hamburg, Germany}

16 [5] {School of Biomedical Sciences, King's College London, London, UK}

17 [6] {School of Earth, Atmospheric and Environmental Sciences, University of
18 Manchester, Manchester, UK}

19 [7] {National Centre for Atmospheric Science, University of Manchester, Manchester,
20 UK}

21 [8] {Aerodyne Research, Inc., Billerica, MA, USA}

22 [9] {Department of Atmospheric Sciences, University of Washington, Seattle, WA,
23 USA}

24 [10] {School of Chemical and Biomolecular Engineering, Georgia Institute of
25 Technology, Atlanta, GA, USA}

26 [11] {School of Earth and Atmospheric Sciences, Georgia Institute of Technology,
27 Atlanta, GA, USA}

28 [12] {Centre for Ecology and Hydrology, Penicuik, Midlothian, Scotland}

29 [13] {Department of Meteorology, University of Reading, Reading, UK}

30 [14] {Department of Chemistry, University of Leicester, Leicester, UK}

1 [*] {now at: European XFEL, Hamburg, Germany}

2 Correspondence to: M. Furger (markus.furger@psi.ch)

3

4 **Abstract**

5 Ambient concentrations of trace elements with 2 h time resolution were measured in
6 $PM_{10-2.5}$, $PM_{2.5-1.0}$ and $PM_{1.0-0.3}$ size ranges at kerbside, urban background and rural
7 sites in London during winter 2012. Samples were collected using rotating drum
8 impactors (RDIs) and subsequently analysed with synchrotron radiation-induced X-
9 ray fluorescence spectrometry (SR-XRF). Quantification of kerb and urban
10 increments (defined as kerb-to-urban and urban-to-rural concentration ratios,
11 respectively), and assessment of diurnal and weekly variability provided insight into
12 sources governing urban air quality and the effects of urban micro-environments on
13 human exposure. Traffic-related elements yielded the highest kerb increments, with
14 values in the range of 10.4 to 16.6 for SW winds (3.3-6.9 for NE) observed for
15 elements influenced by brake wear (e.g. Cu, Sb, Ba) and 5.7 to 8.2 for SW (2.6-3.0
16 for NE) for other traffic-related processes (e.g. Cr, Fe, Zn). Kerb increments for these
17 elements were highest in the $PM_{10-2.5}$ mass fraction, roughly 2 times that of the $PM_{1.0-}$
18 $_{0.3}$ fraction. These elements also showed the highest urban increments (~ 3.0),
19 although no difference was observed between brake wear and other traffic-related
20 elements. All elements influenced by traffic exhibited higher concentrations during
21 morning and evening rush hour, and on weekdays compared to weekends, with the
22 strongest trends observed at the kerbside site, and additionally enhanced by winds
23 coming directly from the road, consistent with street canyon effects. Elements related
24 to mineral dust (e.g. Al, Si, Ca, Sr) showed significant influences from traffic-induced
25 resuspension, as evidenced by moderate kerb (3.4-5.4 for SW, 1.7-2.3 for NE) and
26 urban (~ 2) increments and increased concentrations during peak traffic flow.
27 Elements related to regional transport showed no significant enhancement at kerb or
28 urban sites, with the exception of $PM_{10-2.5}$ sea salt (factor of up to 2), which may be
29 influenced by traffic-induced resuspension of sea and/or road salt. Heavy duty
30 vehicles appeared to have a larger effect than passenger vehicles on the
31 concentrations of all elements influenced by resuspension (including sea salt) and
32 wearing processes. Trace element concentrations in London were influenced by both
33 local and regional sources, with coarse and intermediate fractions dominated by
34 traffic-induced resuspension and wearing processes and fine particles influenced by
35 regional transport.

1

2 **1 Introduction**

3 Ambient particulate matter (PM) has long been recognized to have a detrimental
4 effect on public health in urban areas (e.g. Dockery and Pope, 1994). Of particular
5 interest are particles with an aerodynamic diameter less than 10 μm (PM_{10}) as these
6 particles can penetrate deeply into the lungs (Franklin et al., 2008; Zhou et al., 2011).
7 Reche et al. (2012) reported even higher toxicity to human cells for the $\text{PM}_{2.5-1.0}$ than
8 for the $\text{PM}_{10-2.5}$ fraction. Particle toxicity is known to vary significantly with PM
9 composition and emission sources (Kelly and Fussell, 2012), with identified toxic
10 constituents including soluble secondary inorganic particles, elemental and organic
11 carbon, and especially metals. Effective mitigation strategies therefore require
12 detailed, size-dependent characterization of particle composition and emission
13 sources.

14 In addition to their direct effects on human health, metals and trace elements are of
15 importance because their high source specificity and atmospheric stability make
16 them effective tracers for source apportionment. In Europe, four main source types in
17 PM_{10} are commonly identified: vehicles (with tracers including e.g. Fe, Ba, Zn, Cu),
18 crustal materials (e.g. Al, Si, Ca, Fe), sea salt (mainly Na, Cl, Mg) and mixed
19 industrial/fuel-oil combustion (mainly V, Ni, S) and secondary aerosol (mainly S)
20 (Putaud et al., 2010; Viana et al., 2008). The contribution of mineral dust and sea salt
21 in most urban areas is larger in PM_{10} than in $\text{PM}_{2.5}$ (Harrison et al., 2001; Weijers et
22 al., 2011). Emissions from vehicle exhaust, industry and secondary aerosol are
23 predominantly emitted and formed as $\text{PM}_{1.0}$ or in $\text{PM}_{2.5}$ (Bukowiecki et al., 2010;
24 Harrison et al., 2011; Richard et al., 2011). Several of these sources have been
25 directly linked to adverse health effects. For example, the largest aerosol source of
26 human toxicity in Barcelona was attributed to traffic activities (encompassing vehicle
27 emissions, road dust and secondary nitrate), with fuel oil combustion and industrial
28 emissions also contributing to increased cancer risk (Reche et al., 2012). Turoczi et
29 al. (2012) observed higher toxicity from direct emissions (e.g. from traffic) than from
30 photochemically processed aerosol.

31 The Clean Air for London project (ClearfLo; www.clearflo.ac.uk) is a multinational
32 effort to elucidate the processes driving poor air quality in London, implemented
33 through comprehensive measurements of particle- and gas-phase composition, and
34 meteorological parameters (Bohnenstengel et al., 2014). ClearfLo builds upon recent
35 modelling and monitoring studies in London (Arnold et al., 2004; Bohnenstengel et
36 al., 2011; Bohnenstengel et al., 2013; Harrison et al., 2012a; Mavrogianni et al.,

1 2011). Despite improved air quality, PM_{10} concentrations are not decreasing,
2 resulting in frequent exceedances of the daily PM_{10} limit (Harrison et al., 2008). Such
3 exceedances are caused by complex interactions of regional and local emission
4 sources, together with meteorological factors such as wind speed, air mass origin,
5 and daily cycles of the atmospheric boundary layer (Charron and Harrison, 2005;
6 Harrison and Jones, 2005; Jones et al., 2010). Currently, emissions by industrial
7 sources and stationary combustion are modest, while traffic is thought to contribute
8 up to 80 % of the total PM_{10} in London, compared to less than 20 % for the entire UK,
9 according to emission inventories between 1970 and 2001 (Dore et al., 2003).

10 The spatial density of emission sources found in typical urban environments leads to
11 elevated particle concentrations compared to nearby rural locations. As an example,
12 buildings may influence local meteorology by restricting air circulation (street canyon
13 effect), producing human exposures that are orders of magnitude higher than those
14 predicted by regional dispersion models (Zhou and Levy, 2008). This provides both
15 acute exposure risk and increased long-term exposure for those passing through
16 regularly, thereby producing a non-negligible impact on public health. To assess the
17 impact of such micro-environments, we here investigate London trace element
18 concentrations in terms of increments, defined as the concentration ratios between
19 an environment of interest and a reference site (e.g. Charron et al., 2007).

20 Only a few studies have investigated trace elements through simultaneous
21 measurements at multiple sites. Harrison et al. (2012b) reported increments of
22 kerbside to urban background sites in London for non-size segregated aerosol with a
23 time resolution of 1 to 4 days. Theodosi et al. (2011) found that at urban and
24 suburban sites in Athens and a regional site in Finokalia, Greece crustal elements
25 dominate coarse particles ($PM_{10-2.5}$), whereas anthropogenic sources such as fossil
26 fuel combustion were confined to fine particles (V, Ni and Pb have > 70 % of their
27 mass in $PM_{1.0}$). Bukowiecki et al. (2009a) and Bukowiecki et al. (2010) examined
28 trace elements in $PM_{10-2.5}$, $PM_{2.5-1.0}$ and $PM_{1.0-0.1}$ aerosol at street canyon and urban
29 background sites in Zürich, Switzerland, and showed increasing increments (note: 1
30 means no increment) with particle size from about 1.2 (fine mode) to 2.4 (coarse
31 mode) (averaged over all elements). All these studies report increments close to 1 for
32 elements originating from regional sources such as sea salt and Saharan dust, while
33 local, especially traffic-related sources yield increments around 2 for resuspension-
34 related elements and between 3 and 5 for traffic-related elements. Additionally, the 1
35 h time resolution used by Bukowiecki et al. (2009a) and Bukowiecki et al. (2010)
36 enabled identification of enhanced increments for resuspension and wearing related
37 elements like Si and Sb during peak traffic flows.

1 There is a need for more high time-resolved size segregated increment analyses to
2 assess the exposure to trace elements from emission sources within urban areas
3 under varying meteorological conditions. Here we present size segregated
4 measurements of aerosol trace elements with 2 h time resolution performed
5 simultaneously at kerbside and urban background sites in London, and a rural site
6 outside London. We assess the effects of urban micro-environments on human
7 exposure to particulate pollutants through the quantification of urban and kerb
8 increments. These exposures are further investigated in terms of contributing
9 emission sources, diurnal and weekly variability, local wind patterns, and regional
10 transport effects.

11

12 **2 Methods**

13 **2.1 Measurement campaigns**

14 The ClearLo project was a measurement program in and around London lasting two
15 years (2011-2012) and including two month-long Intensive Observation Periods
16 (IOPs) in 2012 (Bohnenstengel et al., 2014). This paper focuses on the winter IOP
17 lasting from 6 January to 11 February 2012. Measurements took place at three
18 sampling sites located at or near permanent air quality measurement stations in the
19 Automatic Urban and Rural Network (AURN): a kerbside site close to a very busy
20 road, an urban background site in a residential area, and a rural background site
21 away from direct emission sources (see Fig. 1).

22 The urban background sampling site was at the grounds of the Sion Manning
23 Secondary School in North Kensington (NK, lat 51°31'21"N, lon 0°12'49"W). NK is
24 situated within a highly trafficked suburban area of London (Bigi and Harrison, 2010;
25 Harrison et al., 2012a). During the ClearLo IOPs this site served as the main
26 measurement site and was upgraded with a full suite of particle- and gas-phase
27 instruments, and instruments to measure meteorological parameters (Bohnenstengel
28 et al., 2014). The kerbside site was located at Marylebone Road (MR, lat 51°31'21"N,
29 lon 0°09'17"W) about 4.1 km to the east of NK (Charron and Harrison, 2005;
30 Harrison et al., 2011). This site is located at the southern side of a street canyon, with
31 an axis running approximately 260° to 80°. Measurements took place at 1 m from a
32 busy six-lane road with a traffic flow of approximately 73 000 vehicles per day of
33 which 15 % consist of heavy duty vehicles. Braking and stationary vehicle queues
34 are frequent at the site due to a heavily used pedestrian light-controlled crossing (65
35 m west of MR) and a signal-controlled junction (200 m west of MR). The rural site at

1 the Kent Showgrounds at Detling (DE, lat 51°18'07"N, lon 0°35'22"E) was
2 approximately 45 km to the southeast of London downtown on a plateau at 200 m
3 a.s.l. surrounded by fields and villages, and was close to the permanent
4 measurement station of Kent and Medway Air Quality Monitoring Network. The site
5 provides excellent opportunities to compare the urban and kerbside air pollution with
6 the rural background pollution levels (Bohnenstengel et al., 2014; Mohr et al., 2013).
7 A busy road with ~ 160 000 vehicles per day is located approximately 150 m south of
8 DE. Meteorological parameters were measured at DE and at the British Telecom
9 (BT) Tower (lat 51°31'17"N, lon 0°08'20"W), ~ 0.5 km east of MR (Harrison et al.,
10 2012a).

11

12 **2.2 Instrumentation**

13 **2.2.1 RDI-SR-XRF**

14 **Rotating drum impactors**

15 Rotating drum impactors (RDIs) were deployed at MR, NK and DE with a 2 h time
16 resolution (see Table 1 for details). A detailed description of the RDI can be found in
17 Bukowiecki et al. (2005), Bukowiecki et al. (2009c) and Richard et al. (2010). In short,
18 aerosols are sampled through an inlet that removes all particles with aerodynamic
19 diameter $d > 10 \mu\text{m}$ at a flow rate of $1 \text{ m}^3 \text{ h}^{-1}$. The particles are size segregated in
20 three size ranges based on d ($\text{PM}_{10-2.5}$ (coarse), $\text{PM}_{2.5-1.0}$ (intermediate) and $\text{PM}_{1.0-0.3}$
21 (fine)) by passing sequentially through three rectangular nozzles of decreasing size.
22 Particle deposition occurs via impaction on $6 \mu\text{m}$ thick polypropylene (PP) foils
23 mounted on aluminium wheels and coated with Apiezon to minimize particle
24 bouncing effects. After the last impaction stage a backup filter samples all remaining
25 particles before the air passes through a pump. After each 2 h sampling interval the
26 three wheels rotate stepwise to a blank section of the foil before a new sampling
27 interval takes place. The small-size collection limit of the fine fraction was previously
28 estimated at 100 nm (Bukowiecki et al., 2009c; Richard et al., 2010). However, new
29 laboratory measurements of the RDI collection efficiency indicate an instrument-
30 dependent (i.e. based on the machining of the specific nozzle) small-end cut point of
31 approximately 290-410 nm (see Supplement A for details). This results in sampling of
32 a smaller size range ($\text{PM}_{1.0-0.3}$) than the $\text{PM}_{1.0-0.1}$ range reported in previous studies,
33 and influences the measured concentrations of elements with significant mass near
34 this cut point (S, K and Pb).

1

2 **SR-XRF analysis**

3 Trace element analysis on the RDI samples was performed with synchrotron
4 radiation-induced X-ray fluorescence spectrometry (SR-XRF) at the X05DA beamline
5 (Flechsig et al., 2009) at the Swiss Light Source (SLS) at Paul Scherrer Institute
6 (PSI), Villigen PSI, Switzerland and at Beamline L at Hamburger
7 Synchrotronstrahlungslabor (HASYLAB) at Deutsches Elektronen-Synchrotron
8 (DESY), Hamburg, Germany (beamline dismantled November 2012). The samples
9 with the deposited particles were placed directly into the X-ray beam. Irradiation of
10 the samples took place at a 45° angle for 30 s. The light spot of the incoming beam
11 was ~ 140 by 70 μm at SLS (monochromatic excitation at 10.5 keV, in vacuum) and
12 ~ 80 by 150 μm at HASYLAB (polychromatic excitation, in air). Fluorescence light
13 produced by the elements in the samples was detected by energy-dispersive
14 detectors (silicon drift detector at SLS, nitrogen cooled Si(Li)-detector at HASYLAB)
15 at a 90° angle relative to the incoming beam. At SLS Kα lines of the elements with
16 atomic number $Z = 11-30$ (Na-Zn) were measured, and at HASYLAB Kα lines of the
17 elements with $Z = 22-56$ (Ti-Ba) and Lα lines of $Z = 82$ (Pb).

18 The fluorescence counts per element were calibrated to the element mass
19 concentration using multi-element standards, where each standard consisted of a set
20 of preselected elements in 5 different concentrations ranging between 0.05 and 0.4
21 μg cm⁻². The absolute element concentrations in these standards were determined
22 with inductively coupled plasma-optical emission spectroscopy (ICP-OES). The
23 absolute calibration factor for the SR-XRF system was referenced to Fe and
24 determined from the linear relation between the SR-XRF response and the ICP-OES
25 measurements. Because the fluorescence yield increases with atomic number Z , a
26 relative calibration curve was constructed as follows: for each element present in the
27 standards and having a detectable Kα₁ line, an absolute calibration factor was
28 determined as for Fe, and a dimensionless relative response factor was calculated as
29 the ratio of this absolute factor to that of Fe. These relative response factors were
30 plotted as a function of line energy and a polynomial curve was fit to obtain response
31 factors by interpolation for elements not present in the standard. In total 25 elements
32 were quantified (Na, Mg, Al, Si, P, S, Cl, K, Ca, Ti, V, Cr, Mn, Fe, Ni, Cu, Zn, Br, Sr,
33 Zr, Mo, Sn, Sb, Ba, Pb). Details of the methodology can be found elsewhere
34 (Bukowiecki et al., 2005; Bukowiecki et al., 2008; Richard et al., 2010), with the
35 following significant changes (see Supplement B for further details):

1 1. At SLS, we used an e2v SiriusSD detector (SiriusSD-30133LE-IS) and in-house
2 built vacuum chamber to extend the measured range of elements down to Na and
3 Mg.

4 2. Reference standards for calibration of element fluorescence counts to mass
5 concentrations were produced on the same 6 μm PP substrate as used for RDI
6 sampling allowing the use of identical geometry and irradiation time for RDI samples
7 and reference standards, thereby reducing uncertainties in absolute and relative
8 calibrations.

9 3. Data were processed with the Spectral Analysis for Multiple Instruments – toolkit
10 for XRF (SAMI-XRF) developed in-house within the Igor Pro software environment
11 (Wavemetrics, Inc., Portland, OR, USA). SAMI handles spectral fitting, quantification
12 of associated uncertainties, and calculation and application of calibration parameters.

13 XRF is sensitive to self-attenuation of fluorescence radiation in the sample and
14 depends on the sample composition and density, as well as particle layer thickness
15 or particle size. The PM sample thickness of the coarse and intermediate fractions
16 was maximally 0.7-1.5 μm at a maximum concentration of 10 $\mu\text{g m}^{-3}$ total PM mass
17 for each sample. For these fractions, self-absorption therefore mainly occurs within
18 the individual particles (geometric mean of 5 and 1.6 μm for $\text{PM}_{10-2.5}$ and $\text{PM}_{2.5-1.0}$
19 fractions, respectively). For the fine fraction the PM layer is several micrometres
20 thick, resulting in absorption inside the PM layer. However, this layer is mainly
21 composed of species not resolved by SR-XRF (H, C, N, O). Furthermore, most mass
22 of the lightest elements (Na-Ca) is restricted to the coarse and intermediate fractions
23 (except for S and K). We therefore neglect self-absorption effects in the fine fraction
24 samples. The calculated layer thickness of the dried calibration solution on the
25 calibration standards is negligible at 3-60 nm, but the particle size of the dried
26 droplets shows a geometric mean volume size distribution of $9 \pm 5 \mu\text{m}$ and is
27 therefore relevant for self-attenuation. Attenuation factors (AF) were calculated for
28 the calibration standards as well as for the coarse and intermediate fraction samples,
29 as a function of density, mass attenuation coefficient and particle size, according to a
30 simple attenuation model (Table 2; Formenti et al., 2010). For ambient samples and
31 calibration standards, the attenuation length or penetration depth of X-rays for the
32 heavier elements (i.e. above Ca) is greater than 33 μm , resulting in the near-
33 complete excitation of these elements and correction factors below 3 %. Self-
34 absorption correction factors for Na-Ca are non-negligible, as discussed below and in
35 Table 2. The attenuation of the calibration standards is taken into account for all
36 samples, and additional corrections are applied to the coarse and intermediate

1 samples. Calzolari et al. (2010) found comparable self-absorption effects for samples
2 of different composition, total loading and sampling site. Because the elemental
3 composition and particle size distribution of each sample are unknown, we assume a
4 uniform correction for each element within a given size fraction. The overall AF for Na
5 to Ca are 0.52-0.87, 0.30-0.84 and 0.22-0.82 for coarse, intermediate and fine
6 fraction samples, respectively.”

7

8 **2.2.2 Other measurements**

9 Here a short description is given of relevant particle- and gas-phase instruments
10 deployed at MR, NK and DE during the winter IOP. Daily PM₁₀ filter samples
11 (midnight to midnight) were collected at MR and NK using Partisol 2025 samplers
12 (Thermo Scientific, Inc.). The filters were digested in a 1:2 mixture of perchloric and
13 hydrofluoric acid, and subsequently analysed by ICP-mass spectrometry (ICP-MS,
14 calibration with NIST standards) for the determination of Na, Al, Ca, Ti, V, Mn, Fe, Ni,
15 Cu, Zn, Sr, Mo, Sb, Ba and Pb. Additionally, Mg, K and Sn were available at NK.
16 High-resolution time-of-flight aerosol mass spectrometers (HR-ToF-AMS, Aerodyne
17 Research, Inc., Billerica, MA, USA) were deployed at MR (5 min time resolution), NK
18 (5 min resolution every 30 min), and DE (2 min resolution) to characterise the non-
19 refractory submicron aerosol components (DeCarlo et al., 2006). PM₁₀ mass
20 concentrations were measured at all three sites with FDMS-TEOM (Filter Dynamics
21 Measurement System Tapered Element Oscillating Microbalances; Thermo
22 Scientific, Inc.) with a 1 h time resolution. NO_x measurements at MR and NK were
23 performed with a NO_x chemiluminescent analyser with a single chamber and a single
24 detector (API, A Series, model M200A; 15 min resolution). At DE NO was determined
25 with a Thermo Scientific 42i analyser and NO₂ with an Aerodyne CAPS-NO₂ (SN
26 1002) and an Aerodyne QCL-76-D. These NO and NO₂ measurements were
27 summed together to obtain NO_x (1 min resolution). Black carbon (BC) was measured
28 with a 2-wavelength Aethalometer ($\lambda = 370$ and 880 nm, model AE22, Magee
29 Scientific) at MR and a 7-wavelength Aethalometer ($\lambda = 370-950$ nm, model AE31,
30 Magee Scientific) at NK and DE (5 min resolution), with a 2.5 μm cyclone at MR and
31 DE and a 3.5 μm cyclone at NK. Traffic counts by vehicle group at MR from road
32 sensors (number of vehicles per 15 min) were available as well. Wind direction and
33 wind speed data for MR and NK were taken from the BT Tower (30 min resolution)
34 where anemometers were placed to the top of an open lattice scaffolding tower of 18
35 m height on top of the main structure (190.8 m a.g.l.; Wood et al., 2010), whereas

1 local data were used at DE (1 min resolution). Air mass origins were analysed with
2 back trajectory simulations using the UK Met Office's Numerical Atmospheric
3 Modelling Environment (NAME) dispersion model (Jones et al., 2007).

4

5 **3 Data intercomparison and uncertainty**

6 Here we compare RDI-SR-XRF data with independent filter data (24 h PM₁₀ trace
7 element data analysed with ICP-MS; roughly 9 % uncertainty at a 95 % confidence
8 interval) for 18 elements collected at MR and NK (no filter data was available at DE).

9 For this comparison, the three size ranges of the RDI were summed up to total PM₁₀
10 and averaged to the filter collection period. Details of the intercomparison results can
11 be found in Supplement C. In short, the majority of the elements (Al, Ca, Ti, Mn, Fe,
12 Cu, Zn, Sr, Sb, Ba) agree within approximately ± 50 % with Pearson's $R > 0.78$. Na
13 and Mg agree as well, but have higher uncertainties due to self-absorption
14 corrections. For the other elements, disagreement can be attributed to low or
15 unknown filter sample extraction efficiencies (Ni, Mo) and differences in the particle
16 size range sampled by the two measurement techniques (K, V, Sn, Pb). However, all
17 elements are retained in the ensuing analysis as (1) they yield internally consistent
18 results, as described in the following sections; (2) the ensuing analysis relies on
19 relative changes/ratios per element across sites and is therefore not affected by a
20 systematic bias in absolute magnitude.

21 The agreement between XRF and filter measurements in the present study
22 compares favourably with that obtained in previous intercomparisons of trace
23 element measurement techniques. Comparison of RDI-SR-XRF with daily element
24 concentrations from a high volume sampler followed by subsequent analysis using
25 laboratory-based wavelength dispersive XRF (Bukowiecki et al., 2005) and by ICP-
26 OES and ICP-MS (Richard et al., 2010) yielded slopes between 0.7 and 1.6 (except
27 for S and K) with Pearson's $R > 0.5$. The spread/biases in these intercomparisons
28 are not necessarily due to SR-XRF issues, as can be seen from a comparison by
29 Salcedo et al. (2012) of ICP with proton-induced X-ray emission (PIXE) and AMS
30 trace element measurements. Agreement between ICP and PIXE data was in the
31 same range as between either method and the AMS data, with slopes ranging
32 between 0.06 and 0.93 with Pearson's R from about 0.3 to 0.7.

33 Estimated uncertainties (per size fraction) and detection limits for each measured
34 element are given in Supplement Table S3. A brief overview is presented here:

1 1. RDI sampling: the fluctuations in the flow rate are negligible within 5 % (Richard et
2 al., 2010) and the uncertainties in the size cut off are discussed in Supplement A.

3 2. SR-XRF accuracy: uncertainties in the absolute and relative calibrations affect
4 absolute/fractional concentrations, but cancel out for relative changes/ratios, because
5 all samples were measured under the same calibration conditions.

6 3. Issues such as imperfect flatness of the sample foils and detector dead time
7 corrections (Richard et al., 2010) reduce measurement precision but affect all
8 elements with the same scaling factor.

9 4. SR-XRF measurement precision is affected by sample inhomogeneity, spectral
10 analysis and self-absorption correction uncertainties. Sample inhomogeneity was
11 assessed by Bukowiecki et al. (2009c) and found to contribute ± 20 % uncertainty.

12 For most elements, except Mn and the lightest elements, sample inhomogeneity is
13 the largest source of uncertainty. Mn is affected by spectral analysis uncertainties
14 due to peak overlap with Fe, which is present in much higher concentrations.
15 Therefore, a small bias in the energy calibration as function of detector channel leads
16 to a large change in the peak area of Mn. Self-absorption effects are a significant
17 source of uncertainty for the lightest elements (Na-Ca), but the good comparisons to
18 the filter data suggest that the corrections lead to reasonable results. All data points
19 lie well above their element detection limits, resulting in negligible uncertainties from
20 the signal strength. In addition, RDI-SR-XRF measurements (both absolute/fractional
21 and relative/ratio) are affected by atmospheric variability. This variability is likely the
22 predominant source of the data spread evident in Table and the following analyses.

23

24 **4 Results and discussion**

25 **4.1 Trace element concentrations**

26 During the ClearfLo winter IOP total mass concentrations of the analysed trace
27 elements ranged from less than $0.1 \mu\text{g m}^{-3}$ to $\sim 10 \mu\text{g m}^{-3}$. Typically, concentrations
28 were highest at MR and lower at NK and DE, and decreased with particle size. An
29 overview of the obtained trace element concentrations as a function of size and site
30 is given in Table 3. Note that S is not a trace element, but is commonly reported in
31 trace element studies and is a good tracer for regional transport. Among the
32 analysed trace elements, highest concentrations at MR were found for Na (28 %), Cl
33 (25 %) and Fe (22 %). At NK this was the case for Na (39 %), Cl (29 %) and Fe (11

1 %) and at DE Na (40 %), Cl (28 %) and Fe (8 %). Total analysed mass measured by
2 the RDI-SR-XRF (trace elements + S) contributed on average 14 % to the total PM₁₀
3 mass (from FDMS-TEOM) of 32 (5-74) µg m⁻³ at MR (not extrapolated to the
4 corresponding oxides), 10 % to the mass of 23 (1.4-63) µg m⁻³ at NK and 7.4 % to
5 the mass of 17 (0.5-58) µg m⁻³ at DE.

6 A comparison between the contributions of coarse, intermediate and fine fractions to
7 the total PM₁₀ mass of each trace element is shown in Fig. 2 for the three sites. Trace
8 elements at MR are dominated by the coarse fraction. Analysis in the following
9 sections and previous measurements at this site (Charron and Harrison, 2005)
10 suggest this is caused by large contributions of resuspension and traffic-related
11 mechanical abrasion processes, which primarily contribute to the coarse fraction. For
12 all elements at this site, except S, Br and Pb, the coarse fraction contributes more
13 than 50 %. Mass fractions of intermediate mode elements to total PM₁₀ are rather
14 constant with contributions ranging from 11 to 27 %. The fine fraction contributes up
15 to 50 % of total mass for S, K, Zn, Br and Pb; for other elements fine contributions
16 are less than 20 %. S, K, Zn, Br and Pb are typically dominated by the fine fraction
17 with known sources including heavy oil combustion (S, K, Zn; Lucarelli et al., 2000),
18 traffic exhaust (Br, Pb; Formenti et al., 1996), industrial processes (Zn, Pb; Moffet et
19 al., 2008), and secondary sulphate and wood combustion (S, K, Pb; Richard et al.,
20 2011).

21 For most elements, particle mass contributions of the smaller size fractions are more
22 important as one moves from kerbside to urban background to rural sites (Fig. 2).
23 The relatively large fine fraction contribution at DE is probably caused by the
24 absence of local traffic which results in lower contributions of resuspension and
25 traffic-related processes to total element concentrations. A different behaviour is
26 observed for Cr, Ni and Mo with on average 80 % of their mass at DE in the coarse
27 fraction, compared to 73 % at MR and 60 % at NK. The time series of these coarse
28 mode species are very spiky, are slightly enhanced with SW winds, but are not
29 collocated with measurements of BC and AMS species, suggesting emissions from a
30 local industrial source, potentially from stainless steel production (Querol et al., 2007;
31 Witt et al., 2010) near DE rather than regional transport.

32 Comparing the contributions of groups of elements to total trace element
33 concentrations at the sites provides an overview of local and regional sources
34 affecting London; a detailed source apportionment study will be the subject of a
35 future manuscript. Na, Mg and Cl are typical sea salt elements and contribute around
36 66 % to the total PM₁₀ trace element mass at all three sites, indicating that the air

1 pollutant levels caused by elements are dominated by natural emission sources
2 being transported to London. Mineral dust elements (Al, Si, Ca, Ti) mainly brought
3 into the air via resuspension contribute on average 13 % at MR, NK and DE. For
4 some specific brake wear elements (Cu, Sb, Ba) these contributions are 1.5, 0.6 and
5 0.4 % at MR, NK and DE, respectively. Although these metals contribute a small
6 fraction of total PM₁₀ mass concentrations, they induce adverse health effects. Xiao
7 et al. (2013) e.g. found that Zn, Fe, Pb and Mn were the major elements responsible
8 for plasmid DNA damage, whereas Kelly and Fussell (2012) found that increases in
9 PM₁₀ as a result of increased Ni, V, Zn and Cu contributions showed highest mortality
10 risks, as opposed to increased Al and Si.

11

12 **4.2 Urban and kerb increment**

13 **4.2.1 Urban increment**

14 The urban increment compares the trace element concentrations at the urban
15 background site to the concentrations at the rural site, and is calculated here as the
16 ratio of concentrations at NK to DE. Figure 3 shows the mean, median and 25-75th
17 percentile urban increment ratios for the coarse, intermediate and fine fractions per
18 element. Most elements, except Ni and coarse mode Cr are enriched at the urban
19 background site by factors between 1.0 and 6.5 (median ratios). Increments
20 decrease towards smaller sizes. Ni and coarse mode Cr show higher concentrations
21 at DE relative to NK, as does the mean value of coarse Mo. Especially at DE Cr and
22 Ni show strong correlations with Pearson's *R* of 0.85. As discussed in the previous
23 section, enhanced coarse mode Cr, Ni and Mo may indicate an industrial source near
24 the rural site.

25 Coarse mode Zr exhibits low concentrations at DE, where the median value actually
26 falls below detection limit, though discrete events above detection limit also exist. For
27 this reason, the median-based urban increment is not plotted, while the mean ratio is
28 driven by several large concentration peaks at NK, resulting in a large mean ratio of
29 21. In the case of Cl, a large spread in the urban increment values is seen for all
30 three size ranges. Cl is likely depleted relative to other sea salt elements like Na and
31 Mg (throughout the campaign Cl concentrations fall to 0, whereas Na and Mg
32 concentrations remain positive) due to replacement by nitrate, and the extent of such
33 depletion is greater in small particles (Nolte et al., 2008). At DE, Cl depletion seems
34 apparent at all size ranges, whereas at MR depletion mainly takes place in the PM_{1.0-}

1 _{0.3} fraction. NK shows Cl depletion especially in the PM_{1.0-0.3} fraction, but to some
2 extent also in intermediate mode particles.

3 For ease of discussion, we empirically group elements based on similar urban
4 increment values. Mn, Fe, Cu, Zn, Zr, Mo, Sn, Sb and Ba show urban increments on
5 average of 3.5 in the coarse, 3.1 in the intermediate and 2.0 in the fine fraction (Fig.
6 3). These have been identified as traffic-related elements by e.g. Amato et al. (2011);
7 Bukowiecki et al. (2010); Minguillón et al. (2014); Richard et al. (2011) and Viana et
8 al. (2008). Zr has also been linked to mineral dust (Moreno et al., 2013). We can
9 understand that from analysing the Enrichment Factors of these elements (EF). EF is
10 a measure of the enrichment of elements relative to the upper continental crust
11 (UCC) and is defined as ppm metal in the sample / ppm metal in UCC with Si as
12 reference material (UCC from Wedepohl, 1995). Zr is the only element in this traffic
13 group that is depleted in the atmosphere relative to their UCC concentrations, but
14 with concentrations at NK higher than at DE. Most other elements clearly indicate
15 anthropogenic origin with EF > 10. Dependent on the method, Zr can be either
16 grouped with traffic-related elements or with dust elements. The urban increments
17 are similar to that of NO_x, where concentrations at NK were on average a factor 4.9
18 higher than at DE (the mean concentration at NK was 68 ppb, at DE 14 ppb). Black
19 carbon (BC), a marker for both traffic and wood burning emissions, had an urban
20 increment of only 1.1 (concentration at NK 757 ng m⁻³, at DE 633 ng m⁻³), likely due
21 to local wood burning emissions around DE (Mohr et al., 2013). Al, Si, Ca, Ti and Sr
22 as markers for mineral dust (e.g. Amato et al., 2009; Lin et al., 2005; Lucarelli et al.,
23 2000) show a factor 2.0 higher concentrations at NK relative to DE in the coarse, 1.9
24 in the intermediate and 1.6 in the fine fraction (EF < 10). These results indicate that
25 moving from rural to urban backgrounds yields a larger relative increase in traffic
26 than in mineral dust elements. Surprisingly, sea salt elements (Na, Mg, Cl) show
27 higher concentrations at NK than at DE of up to a factor of 2 for the coarse mode,
28 despite the expected dominance of regional over local sources. This highlights the
29 potential importance of sea or road salt resuspension by traffic. Similar urban
30 increment values for traffic-related, resuspension and sea salt elements have been
31 observed by Lee et al. (1994) for particles below a few µm. Theodosi et al. (2011)
32 also found higher increments (> 2) for trace elements in PM₁₀ aerosol from local
33 anthropogenic sources like fossil fuel combustion (V, Ni, Cd) and traffic (Cu), relative
34 to long-range transported Saharan dust (Fe, Mn) with increments close to 1.
35 However, our study suggests that the non-size-resolved increment values reported in
36 the cited studies do not fully capture the urban/rural differences.

1 The influence of regional transport by anthropogenically produced elements (Fig. 3)
2 is seen by the low urban increments between 1.1 and 1.8 for P, S, K, Zn, Br, Sn and
3 Pb in $PM_{1.0-0.3}$ (EF > 22) and of 1.6 for total PM_{10} mass (concentration at NK $23 \mu\text{g m}^{-3}$,
4 3 , at DE $17 \mu\text{g m}^{-3}$). The concentrations of the main components in PM_{10} (sulphate,
5 nitrate and secondary organic compounds) within an urban area are mostly
6 influenced by regional transport, as found in London during the REPARTEE project
7 (Harrison et al., 2012a) and in Paris during the MEGAPOLI project (Crippa et al.,
8 2013; Freutel et al., 2013), resulting in low increments for total PM_{10} mass. Similar
9 urban increment values (1.3 to 1.8) for 1 and 24 h total $PM_{2.5}$ mass concentrations
10 were reported across many sites in the UK (Harrison et al., 2012c).

11

12 **4.2.2 Kerb increment**

13 While the urban increment investigates the effect of diffuse emission sources on
14 particle concentrations, the kerb increment investigates an urban micro-environment,
15 specifically the local effects of roadside emissions and activities. Here, the kerb
16 increment is calculated as the ratio of concentrations at MR to NK. However,
17 observed concentrations at MR strongly depend on wind direction, because the road
18 runs from approximately 260° to 80° and the street canyon with the surrounding
19 buildings and intersections creates a complex wind circulation system (Balogun et al.,
20 2010). Since the measurement station is located at the southern side of the canyon,
21 measurements during time periods with winds from the south are influenced by on-
22 road emissions on top of the urban background pollution. Higher concentrations were
23 observed with SSE winds, i.e. perpendicular to the direction of the road by e.g.
24 Balogun et al. (2010), Charron and Harrison (2005) and Harrison et al. (2012b).

25 In this study, the RDI-SR-XRF data was split into four equally spaced wind direction
26 sectors based on wind direction data; N ($315-45^\circ$), E ($45-135^\circ$), S ($135-225^\circ$) and W
27 ($225-315^\circ$). Figure 4 shows size-resolved trace element concentrations per wind
28 sector normalized to the global median concentration for each element at MR. As
29 expected, winds from the south yield the highest concentrations, whereas northern
30 winds yield the lowest, independent of size fraction. West and east winds are parallel
31 to the street canyon and yield intermediate concentrations. Similar behaviour is
32 observed for NO_x , and no directional biases for high wind speeds are observed
33 (Supplement Fig. S6).

34 Traffic-related and some other anthropogenically-related elements (V, Cr, Mn, Fe, Ni,
35 Cu, Zn, Zr, Mo, Sn, Sb, Ba) show the strongest wind direction dependency with up to

1 a factor of 2-3 higher concentrations during S relative to N winds for the three size
2 fractions (Fig. 4). A factor of 1.5-2 is obtained for resuspended dust elements.
3 Harrison et al. (2012b) found a ratio of 2 for Fe (as tracer for brake wear) and 1.2 for
4 Al (as tracer for mineral dust) for SW versus NE winds for particles between 2 and 3
5 μm . However, they were limited by their time resolution of several days, resulting in
6 potentially substantial wind direction variations during each measurement, which
7 would blur the different conditions and yield reduced ratios.

8 Other elements show only minor correlations with wind direction (Fig. 4), indicating
9 more influence from regional transport, instead of being locally affected by traffic.
10 Only fine mode S, K and Br seem to be enriched with winds from the east, potentially
11 related to long-range transport from the European continent.

12 Local wind direction has a greatly reduced effect at urban background and rural sites.
13 At NK, the element concentrations are only subject to high concentration outliers for
14 E winds (Supplement Fig. S4), potentially caused by the transport of pollutants from
15 downtown London, or by lower wind speeds occurring with E winds resulting in
16 reduced dilution and increased concentrations of traffic pollutants (e.g. NO_x)
17 throughout the city (Supplement Fig. S6). The rural site hardly shows wind direction
18 dependent concentrations (Supplement Fig. S5-6). Interpretation of data from the E
19 sector is unclear due to the low number of data points (45 out of 318 data points).
20 Only data from the N sector show enhanced concentrations for several elements
21 correlating with higher wind speeds and back trajectories consistent with transport
22 from continental Europe.

23 To simplify reporting of the kerb increment and facilitate comparison with previous
24 studies (e.g. Harrison et al., 2012b), we combined the south/west sectors and the
25 north/east sectors into SW ($135\text{-}315^\circ$) and NE ($315\text{-}135^\circ$) sectors. To eliminate
26 meteorological and/or regional transport effects, this segregation is performed at both
27 MR and NK. The kerb increment is then calculated as the ratio of MR to NK and
28 shown in Fig. 5 (Supplement Fig. S7 shows the increments for the 4 individual
29 sectors). As with the urban increment, we focus on the ratio of the medians at MR
30 and NK to reduce the effects of outliers. Two features become directly visible; the
31 kerb increment is much higher for coarse than for intermediate and fine particles, and
32 kerb increments are much higher for SW than for NE wind conditions. With the latter,
33 kerb increments are on average 2.7, 1.6 and 1.7 for coarse, intermediate and fine
34 mode particles, respectively. This significant enhancement is likely due to
35 recirculation of particles within the street canyon following their resuspension and/or

1 emission by traffic. However, these increments are much smaller than those
2 observed in the SW sector, where enhancements relative to NK of 6.7, 3.3 and 3.1
3 (coarse, intermediate, fine) are observed. These results indicate the existence of
4 micro-environments within the street canyon dependent on wind direction.

5 As in the previous discussion, we again group elements by kerb increment (Fig. 5).
6 The first group consists of Cu, Zr, Mo, Sn, Sb and Ba and yields the highest
7 increments in the coarse mode ranging from 10.4 to 16.6 in the SW sector (3.3-6.9
8 for NE). These elements are typically associated with brake wear (e.g. Bukowiecki et
9 al., 2009b; Harrison et al., 2012b), and are much higher than the increments of 4.1 to
10 4.4 reported by Harrison et al. (2012b) at the same sites for particles < 21 μm . They
11 assigned Fe, Cu, Sb and Ba to brake wear, but in the current study Fe has a
12 significantly lower kerb increment than other brake wear tracers, suggesting a
13 significant alternative source. When combining all size fractions and ignoring wind
14 direction influences, increments in this study are about 4.9, and more similar to
15 previous studies. The discrepancies between the kerb increments obtained using
16 these two calculation strategies highlights the difficulties in characterizing human
17 exposure to locally generated pollutants in urban environments, as the detailed
18 topography and microscale meteorology greatly alter particle concentrations, and the
19 effects are size-dependent. Amato et al. (2011) calculated road side increments in
20 Barcelona for trace elements in PM_{10} with a 1 h time resolution and found increments
21 for brake wear elements of only 1.7 (based on Fe, Cu, Sb, Cr, Sn). These low
22 increments are probably due to the reduced dispersion in Barcelona caused by a
23 complex topography, resulting in high urban background levels.

24 The second group consists of V, Cr, Mn, Fe, Ni, Zn and Pb with increments of 5.7-8.2
25 ($\text{PM}_{10-2.5}$) in the SW sector (2.6-3.0 for NE) (Fig. 5). V and Ni are typically assigned to
26 industrial sources and heavy-oil combustion (e.g. Mazzei et al., 2007; Viana et al.,
27 2008), Zn is usually associated with tire wear (e.g. Harrison et al., 2012b; Lin et al.,
28 2005), and the other elements are commonly associated with traffic-related
29 emissions (e.g. Amato et al., 2013; Bukowiecki et al., 2009a; Richard et al., 2011).
30 We label this group as anthropogenically-influenced (ANTH). The EF of V, Cr and Ni
31 are much lower than those of the other elements in this group (4 vs. > 10), indicating
32 at least to some extent different source origins. These kerb increments are similar to
33 the ones for NO_x of 8.5 for SW and 2.4 for NE, confirming the anthropogenic
34 influence (traffic and other sources) on these elements. The high braking frequency
35 at MR due to congested traffic probably resulted in increased kerb increments of

1 brake wear relative to ANTH elements that are also influenced by local traffic and
2 other sources around NK. Increments of these ANTH elements are higher than
3 previously reported values of 1.8-4.5 for studies with low time resolution and non-size
4 segregated particles (Boogaard et al., 2011; Janssen et al., 1997). The high
5 increments presented here might be caused by street canyon effects, trapping
6 pollutants emitted at street level and preventing dilution to the urban background.
7 The enhanced kerb increments for brake wear relative to ANTH elements are
8 apparent in all three size fractions, although increments become more similar
9 towards smaller sizes with a factor 1.7 between both element groups in the coarse,
10 1.5 in the intermediate and 1.4 in the fine mode. Both groups show the additional
11 information gained with size-segregated aerosol, where exposure to trace elements
12 in the street canyon relative to the urban background increases with particle size,
13 either caused by increased traffic-related emissions with particle size or by more
14 efficient transport of submicron particles from street sites to the urban background.
15 Furthermore, the highly time-resolved element measurements presented here
16 enabled us to resolve the systematic, wind direction dependent variability in kerb
17 increments.

18 The third group is associated with mineral dust (Al, Si, Ca, Ti, Sr) with coarse mode
19 increments of 3.4-5.4 for SW winds (1.7-2.3 for NE) (Fig. 5). These elements are
20 brought into the air both by traffic-induced resuspension and transport from other
21 locations. This second process increases both urban background and kerbside
22 concentrations, and thus reduces kerb increments relative to direct traffic-related
23 elements. Lower kerb increments for mineral dust than traffic-related elements are
24 generally observed in increment studies (Amato et al., 2011; Boogaard et al., 2011;
25 Bukowiecki et al., 2009b; Harrison et al., 2012b), although the dust increments found
26 in this study are larger than most reported increments (typically 1-2). As in the traffic-
27 related groups, increments increase with particle size, indicating enhanced human
28 exposure at the street side of particles above 1 μm .

29 Na, Mg and Cl (sea salt) form the fourth group and yield kerb increments of 1.0 to
30 2.7, independent of size fraction but with slightly enhanced ratios with SW compared
31 to NE winds (Fig. 5). Similar increments were observed for total PM_{10} mass. As
32 discussed for urban increments, even though these elements have regional sources,
33 they are influenced by resuspension processes within the urban area which are
34 enhanced at kerbside sites.

35 The remaining elements (P, S, K, Br) can be grouped together. In the coarse mode,
36 these elements yield increments similar to the mineral dust group, indicating that this

1 group is influenced by resuspension processes in the street canyon (Fig. 5).
2 However, especially in the fine mode increments around 1 were found, consistent
3 with regional transport dominating over local emission sources.

4

5 **4.3 Temporal trends in trace element concentrations**

6 In contrast to traditional trace element measurements, the RDI-SR-XRF enables
7 measurement of element concentrations with high time resolution (2 h in this work).
8 This enables investigation of diurnal cycles, which are useful both for source
9 discrimination and in determining the processes contributing to elevated PM levels.
10 We also discuss weekly cycles, which can be useful in distinguishing emissions from
11 heavy duty and passenger vehicles (HDV and LDV); HDV numbers typically diminish
12 during the weekend. Back trajectory analysis aids source discrimination by
13 understanding regional transport influences by different air mass origin. Here we
14 discuss the temporal trends of trace elements in five groups based on expected
15 sources and the increment analyses in Sect. 4.2, in order of increasing local
16 influence: regional background, sea salt, mineral dust, traffic-related and brake wear.

17 Figures 6 and 7 show size-segregated median diurnal and weekly cycles,
18 respectively, for 5 elements representative of the classes mentioned above: Na (sea
19 salt), Si (mineral dust), S (regional background), Fe (traffic-related) and Sb (brake
20 wear) at the three sites. Because of the wind direction effect evident at MR, diurnal
21 cycles at all three sites are shown for SW and NE winds. Wind direction analyses are
22 not incorporated into the weekly cycles because the month-long campaign provided
23 insufficient data points for meaningful division. This also means that weekly cycles
24 are subject to influences by mesoscale events. For example, sea salt shows no clear
25 weekly cycle, except for a peak on Fridays in intermediate and fine fractions
26 coinciding with westerly winds, which coincidentally occurred more frequently on
27 Fridays than on other days. Except for such events, regionally dominated elements
28 tend to display flat, featureless diurnal/weekly cycles, while elements dominated by
29 recurring local processes (e.g. traffic patterns) show interpretable features. Diurnal
30 and weekly cycles of all other elements can be found in Supplement Fig. S8-9. For
31 comparison, diurnal and weekly cycles of NO_x and total PM₁₀ mass at all sites, and of
32 traffic flow at MR are shown in Fig. 8. The time series of these species were
33 averaged to the RDI collection times before obtaining the cycles. BC diurnal and
34 weekly cycles (not shown) are very similar to those of NO_x.

1

2 **4.3.1 Regional influences**

3 Elements dominated by regional sources (P, S, K, Br) occur mainly in the fine fraction
4 and are similar to total PM₁₀ mass in showing no obvious diurnal and weekly
5 patterns. This interpretation is consistent with the urban/kerb increment analysis
6 discussed in Sect. 4.2. Weekly patterns suggest fine Zn and Pb are also dominated
7 by regional transport (Supplement Fig. S9). P, S and K have been identified as
8 tracers for mixed wood combustion and secondary sulphate (Amato et al., 2011;
9 Richard et al., 2011), whereas Hammond et al. (2008) have identified S, K and Pb
10 from mixed secondary sulphate and coal combustion. Br is usually associated with
11 sea salt (Lee et al., 1994; Mazzei et al., 2007) or traffic emissions (Gotschi et al.,
12 2005; Lee et al., 1994), but Maenhaut (1996) has also found Br, together with S, K,
13 Pb and other elements in biomass burning. In this study, the diurnal cycle of fine Br is
14 different from the Na, Mg and Cl cycles, but more similar to K. Br is thus likely more
15 associated with wood burning than with other sources.

16 The time series of fine S, K, Zn, Pb at NK (very similar at MR and DE) are explored in
17 relation to total PM₁₀ mass, wind direction and air mass origin, and compared to
18 representative elements from the other emission groups (coarse Na, Si, S, Sb; Fig.
19 9). Air mass origin was studied with back trajectories simulated for three case study
20 periods (marine, European mainland and locally influenced) using the NAME model
21 (Jones et al., 2007). Particles are released into the model atmosphere from the
22 measurement location and their origin is tracked using meteorological fields from the
23 Unified Model, a numerical weather prediction model. Each particle carries mass of
24 one or more pollutant species and evolves by various physical and chemical
25 processes during 24 h preceding arrival at NK. Potential emission source regions can
26 be highlighted along the pathway to the measurement site at 0-100 m above ground.

27 Under marine air mass origin (case A, 18-24 January, Fig. 9) with strong W winds the
28 concentrations of the fine mode elements are fairly low, whereas sea salt
29 concentrations are enhanced (see Na in Fig. 9). Although the air mass has also
30 passed over Ireland and the Midlands, the influence of these rather sparsely
31 populated regions on pollution levels seems small. This is confirmed by low total
32 PM₁₀ mass and NO_x concentrations. Enhanced fine fraction and total PM₁₀ mass
33 concentrations (latter not shown) occur during north easterlies with high wind speeds
34 from the European mainland (case B) bringing in pollutants through regional
35 transport.

1 During this episode, both the urban background and rural site observed the highest
2 concentrations for these trace elements of the entire campaign. Traffic influenced
3 species were not enhanced during this pollution episode. Elevated concentrations of
4 all trace elements, NO_x and PM₁₀ mass occurred only during a local pollution episode
5 of roughly 3 days caused by local air mass stagnation over London and the south
6 eastern UK (case C). The very high concentrations observed in case B through
7 regional transport from the European mainland were identified as the main reason for
8 PM₁₀ limit exceedances at urban background sites in London by Charron et al.
9 (2007), while exceedances were much less frequent under marine influenced air as
10 represented by case A in this study.

11

12 **4.3.2 Sea salt**

13 The sea salt group yields comparable, rather flat diurnal cycles for fine and
14 intermediate mode Na, Mg and Cl, and coarse mode Na and Cl (Na in Fig. 6; others
15 in Supplement Fig. S8), and no obvious weekly patterns (Na in Fig. 7; others in
16 Supplement Fig. S9). This indicates that the regional transport of sea salt is probably
17 the main source of Na, Mg and Cl, as seen in case A in Fig. 9.

18 Interestingly, although coarse mode sea salt exhibits no obvious temporal trend, the
19 urban and kerb increments indicate additional source contributions besides regional
20 transported sea salt. The urban increment might be caused by the natural sea salt
21 gradient observed in the UK, with reducing concentrations from west to east (Fowler
22 and Smith, 2000), while the kerb increment could be the result of road salt
23 resuspension in addition to sea salt resuspension. Coarse mode Mg originates
24 probably both from mineral dust and sea salt, because at MR with SW winds Mg
25 correlates with Al and Si temporal trends, while with NE winds Mg correlates better
26 with Na and Cl.

27

28 **4.3.3 Mineral dust and traffic**

29 Both mineral dust and traffic-related elements are strongly influenced by traffic
30 patterns at MR, which are shown in Fig. 8 as the number of vehicles per 2 h split in
31 LDV and HDV (shorter/longer than 5.2 m). HDV numbers peak in the morning,
32 whereas LDV numbers peak in the evening when the flow of traffic leaves the urban
33 area, consistent with Harrison et al. (2012b). A single peak during midday in the
34 weekend compared to a double peak at weekdays is observed for LDV. HDV

1 numbers show a similar pattern during weekdays, but with a reduced maximum on
2 Saturday and a small maximum that is shifted towards midday on Sunday. Charron
3 and Harrison (2005) reported similar traffic patterns during two years of traffic counts,
4 and stated very small week-to-week variability, except during holidays.

5 The element diurnal (Fig. 6 for Si, Fe and Sb; Supplement Fig. S8 for others) and
6 weekly (Fig. 7 for Si, Fe and Sb; Supplement Fig. S9 for others) cycles yield highest
7 concentrations at MR and lower concentrations at NK and DE, consistent with
8 observed urban and kerb increments. More importantly, and only retrievable with
9 high time-resolved data, concentrations are higher during the day than at night, with
10 night time concentrations at MR and NK similar to median urban background and
11 rural concentrations, respectively, demonstrating the effects of local traffic and
12 enhanced human exposure during daytime. Weekdays yield stronger increments
13 than weekends and closely follow NO_x and HDV traffic patterns (Fig. 8), indicating
14 the strong influence of these vehicles on element concentrations. This confirms
15 observations by Charron et al. (2007), who stated that PM₁₀ limit exceedances at MR
16 are more likely to occur on weekdays, in combination with large regional
17 contributions from the European mainland with easterly winds. Similarly,
18 Barmpadimos et al. (2011) found strong weekly cycles for PM_{10-2.5} and PM_{2.5} mass
19 concentrations in Switzerland over a 7-12 year period, with higher concentrations on
20 weekdays and lowest on Sundays.

21 In the street canyon with SW winds, all coarse mode elements (including dust
22 elements) except Na and Cl exhibit a double peak in the diurnal cycles, closely
23 following the flow of traffic and confirming that traffic-related processes such as
24 braking and resuspension dominate the concentration of most elements. With NE
25 winds, source discrimination is possible between mineral dust (Si in Fig. 6) and
26 traffic-related elements (Fe and Sb in Fig. 6). Mineral dust yields a strong maximum
27 between 8:00 and 14:00 LT, and continued high concentrations throughout the day,
28 while the traffic-related group yields a reduced double peak relative to SW winds.
29 The increase in dust concentrations coincides with the start of traffic flows at 6:00 LT
30 resulting in resuspension of particles within the street canyon. However,
31 concentrations decrease before traffic flows reduce, possibly as a result of increased
32 mixing and dilution during boundary layer growth. At NK diurnal and weekly patterns
33 of the dust and traffic groups yield similar variability but reduced concentrations
34 relative to MR, which suggests increased human exposure during day time and
35 weekdays and confirms that traffic dominates urban background element
36 concentrations in London (see Dore et al., 2003). At DE, freshly emitted pollutants

1 from London and other cities in the south eastern UK have been diluted and mixed
2 with other pollutants during their transport to the rural background, resulting in no
3 obvious diurnal and weekly patterns independent of size range.

4 The kerb increments at MR under SW winds were divided into two traffic-related
5 groups: brake wear and other traffic-related elements. However, the diurnal and
6 weekly cycles of all these elements correlate well and no obvious split into two
7 groups is seen. Apparently, both groups are co-emitted as a single group under
8 comparable vehicle fleet and/or set of driving conditions, at least on a 2 h time scale,
9 but in different ratios at MR and NK. The ratio of these two element classes for SW to
10 NE wind sectors at MR is almost 2, with the lack of difference between these classes
11 supporting co-emission. In a future manuscript we will further explore the diurnal
12 variability of emission sources at both sites with statistical analyses based on the
13 Multilinear Engine (Canonaco et al., 2013; Paatero, 1999).

15 **5 Conclusions**

16 Aerosol trace element composition was measured at kerbside, urban background
17 and rural sites in the European megacity of London during winter 2012. Sampling
18 with rotating drum impactors (RDI) and subsequent measurements with synchrotron
19 radiation-induced X-ray fluorescence spectrometry (SR-XRF) yielded trace element
20 mass concentrations in $PM_{10-2.5}$, $PM_{2.5-1.0}$ and $PM_{1.0-0.3}$ aerosol with a 2 h time
21 resolution. Total median element mass concentrations of 4.1, 2.1 and $1.0 \mu g m^{-3}$
22 were found at kerbside, urban background and rural sites, respectively, which
23 constitutes to 14 % to total PM_{10} mass (highest at kerbside; lowest at rural site),
24 neglecting the corresponding oxides. The contribution of emission sources to coarse
25 fraction elements was on average largest at kerbside (65 %) and reduced for urban
26 background (52 %) and rural sites (49 %).

27 Urban and kerb increments were defined as the concentration ratios of urban
28 background to rural, and kerbside to urban background, respectively, and the kerb
29 increments were further explored as a function of wind direction. The group with the
30 largest kerb increments consisted of elements typically associated with brake wear
31 (Cu, Zr, Mo, Sn, Sb, Ba). The second largest kerb increments were observed for
32 anthropogenically-influenced elements typically assigned to non-brake wear traffic
33 emissions (Cr, Mn, Fe, Zn, Pb) but also V and Ni. This could indicate either a traffic
34 source for these elements or a similar kerbside-to-urban emission gradient. Kerb
35 increments were larger for the brake wear group and under SW winds due to local

1 street canyon effects, with coarse fraction increments between 10.4 and 16.6 for SW
2 winds (3.3-6.9 for NE winds) against increments for the anthropogenically-influenced
3 group between 5.7 and 8.2 for SW winds (2.6-3.0 for NE winds). The kerb increments
4 for all these elements in the $PM_{10-2.5}$ size fraction are roughly twice that of the $PM_{1.0-0.3}$
5 fraction. Urban increments (no distinction between both groups) were around 3.0. In
6 addition to direct emissions, traffic-related processes influence the concentrations of
7 other elements by resuspension, with mineral dust (Al, Si, Ca, Ti, Sr) increments of
8 1.3-3.3.

9 The highly time-resolved data enabled studying diurnal patterns. The cycles of
10 mineral dust elements and coarse Na, Mg and Cl both indicate major concentration
11 enhancements during periods of heavy traffic, whereas regionally-influenced
12 elements (fine P, S, K, Zn, Br, Pb) showed no enhancements. All traffic-related
13 elements at the kerbside site yielded temporal patterns similar to variations in heavy
14 duty vehicle numbers as opposed to total vehicle numbers, and resulted in enhanced
15 exposure to elements during day time and weekdays. Traffic-related processes
16 therefore exhibit a dominant influence on air quality at the kerbside and urban
17 background sites, and should be the main focus of health effect studies and
18 mitigation strategies. With technological improvements for the reduction of traffic
19 exhaust emissions, the traffic contribution to coarse PM is becoming more important
20 as shown by decreasing $PM_{2.5}$ mass trends with no significant changes of coarse PM
21 (Barmpadimos et al., 2012).

22 Trace element and total PM_{10} mass concentrations are also affected by mesoscale
23 meteorology, increasing with the transport of air masses from the European
24 mainland. Under these conditions, coarse and intermediate fraction trace elements
25 are hardly affected, but fine fraction elements showed elevated concentrations. Trace
26 element concentrations in London are therefore influenced by both local and regional
27 sources, with coarse and intermediate fractions dominated by anthropogenic
28 activities (particularly traffic-induced resuspension and wearing processes), whereas
29 fine fractions are significantly influenced by regional processes.

30 These observations highlight both the strong influence of regional factors on overall
31 air quality, as well as the need for detailed characterization of urban micro-
32 environments for accurate assessment of human exposure to airborne particulates
33 and the associated health risks.

34

35 **Acknowledgements**

1 This research, which was conducted in the context of the ClearLo project, is mainly
2 financed by the Swiss National Science Foundation (SNSF grant 200021_132467/1),
3 the ClearLo project (NERC grant NE/H00324X/1) and the European Community's
4 Seventh Framework Programme (FP/2007-2013, grant number 312284). The Detling
5 site was supported by the US Department of Energy Atmospheric Systems Research
6 Program (DOE Award No. DE-SC0006002). J.G. Slowik acknowledges support from
7 the SNSF through the Ambizione program (grant PX00P2_31673). Filter digestions
8 were carried out by the wet geochemistry laboratory at Royal Holloway, University of
9 London. Empa loaned us a RDI during the ClearLo project. Parts of the work were
10 carried out at the Swiss Light Source, Paul Scherrer Institute, Villigen, Switzerland.
11 We thank Andreas Jaggi for technical support at the beamline X05DA. Parts were
12 performed at the light source facility DORIS III at HASYLAB/DESY. DESY is a
13 member of the Helmholtz Association (HGF). We thank Christophe Friehe for excellent
14 support in acquiring and testing the detector, and we thank Peter Lienemann and
15 Sylvia Köchli for valuable input for the production of calibration standards.

16

17 **References**

- 18 Amato, F., Pandolfi, M., Escrig, A., Querol, X., Alastuey, A., Pey, J., Perez, N., and
19 Hopke, P. K.: Quantifying road dust resuspension in urban environment by Multilinear
20 Engine: A comparison with PMF2, *Atmos. Env.*, 43, 2770-2780, 2009.
- 21 Amato, F., Viana, M., Richard, A., Furger, M., Prevot, A. S. H., Nava, S., Lucarelli, F.,
22 Bukowiecki, N., Alastuey, A., Reche, C., Moreno, T., Pandolfi, M., Pey, J., and
23 Querol, X.: Size and time-resolved roadside enrichment of atmospheric particulate
24 pollutants, *Atmos. Chem. Phys.*, 11, 2917-2931, 2011.
- 25 Amato, F., Schaap, M., Denier van der Gon, H. A. C., Pandolfi, M., Alastuey, A.,
26 Keuken, M., and Querol, X.: Short-term variability of mineral dust, metals and carbon
27 emission from road dust resuspension, *Atmos. Env.*, 74, 134-140, 2013.
- 28 Arnold, S. J., ApSimon, H., Barlow, J., Belcher, S., Bell, M., Boddy, J. W., Britter, R.,
29 Cheng, H., Clark, R., Colvile, R. N., Dimitroulopoulou, S., Dobre, A., Grealley, B.,
30 Kaur, S., Knights, A., Lawton, T., Makepeace, A., Martin, D., Neophytou, M., Neville,
31 S., Nieuwenhuijsen, M., Nickless, G., Price, C., Robins, A., Shallcross, D.,
32 Simmonds, P., Smalley, R. J., Tate, J., Tomlin, A. S., Wang, H., and Walsh, P.:
33 Introduction to the DAPPLE Air Pollution Project, *Sci. Total Environ.*, 332, 139-153,
34 2004.
- 35 Balogun, A. A., Tomlin, A. S., Wood, C. R., Barlow, J. F., Belcher, S. E., Smalley, R.
36 J., Lingard, J. J. N., Arnold, S. J., Dobre, A., Robins, A. G., Martin, D., and
37 Shallcross, D. E.: In-street wind direction variability in the vicinity of a busy
38 intersection in central London, *Bound.-Layer Meteor.*, 136, 489-513,
39 doi:10.1007/s10546-010-9515-y, 2010.
- 40 Barmpadimos, I., Nufer, M., Oderbolz, D. C., Keller, J., Aksoyoglu, S., Hueglin, C.,
41 Baltensperger, U., and Prévôt, A. S. H.: The weekly cycle of ambient concentrations

1 and traffic emissions of coarse (PM₁₀–PM_{2.5}) atmospheric particles, *Atmos. Env.*,
2 45, 4580-4590, 2011.

3 Barmpadimos, I., Keller, J., Oderbolz, D., Hueglin, C., and Prévôt, A. S. H.: One
4 decade of parallel fine (PM_{2.5}) and coarse (PM₁₀–PM_{2.5}) particulate matter
5 measurements in Europe: trends and variability, *Atmos. Chem. Phys.*, 12, 3189-
6 3203, doi:10.5194/acp-12-3189-2012, 2012.

7 Bigi, A., and Harrison, R. M.: Analysis of the air pollution climate at a central urban
8 background site, *Atmos. Env.*, 44, 2004-2012, 2010.

9 Bohnenstengel, S. I., Evans, S., Clark, P. A., and Belcher, S. E.: Simulations of the
10 London urban heat island, *Quart. J. Roy. Meteorol. Soc.*, 137, 1625-1640,
11 doi:10.1002/qj.855, 2011.

12 Bohnenstengel, S. I., Hamilton, I., Davies, M., and Belcher, S. E.: Impact of
13 anthropogenic heat emissions on London's temperatures, *Quart. J. Roy. Meteorol.*
14 *Soc.*, doi:10.1002/qj.2144, 2013.

15 Bohnenstengel, S. I., Belcher, S. E., Aiken, A., Allan, J. D., Allen, G., Bacak, A.,
16 Bannan, T. J., Barlow, J. F., Beddows, D. C. S., Bloss, W. J., Booth, A. M., Chemel,
17 C., Coceal, O., Di Marco, C. F., Dubey, M. K., Faloon, K. H., Fleming, Z. L., Furger,
18 M., Gietl, J. K., Graves, R. R., Green, D. C., Grimmond, C. S. B., Halios, C. H.,
19 Hamilton, J. F., Harrison, R. M., Heal, M. R., Heard, D. E., Helfter, C., Herndon, S.
20 C., Holmes, R. E., Hopkins, J. R., Jones, A. M., Kelly, F. J., Kotthaus, S., Langford,
21 B., Lee, J. D., Leigh, R. J., Lewis, A. C., Lidster, R. T., Lopez-Hilfiker, F. D.,
22 McQuaid, J. B., Mohr, C., Monks, P. S., Nemitz, E., Ng, N. L., Percival, C. J., Prévôt,
23 A. S. H., Ricketts, H. M. A., Sokhi, R., Stone, D., Thornton, J. A., Tremper, A. H.,
24 Valach, A. C., Visser, S., Whalley, L. K., Williams, L. R., Xu, L., Young, D. E., and
25 Zotter, P.: Meteorology, air quality, and health in London: The ClearLo project, *Bull.*
26 *Am. Meteor. Soc.*, (online release), doi:10.1175/bams-d-12-00245.1, 2014.

27 Boogaard, H., Kos, G. P. A., Weijers, E. P., Janssen, N. A. H., Fischer, P. H., van der
28 Zee, S. C., de Hartog, J. J., and Hoek, G.: Contrast in air pollution components
29 between major streets and background locations: Particulate matter mass, black
30 carbon, elemental composition, nitrogen oxide and ultrafine particle number, *Atmos.*
31 *Env.*, 45, 650-658, 2011.

32 Bukowiecki, N., Hill, M., Gehrig, R., Zwicky, C. N., Lienemann, P., Hegedus, F.,
33 Falkenberg, G., Weingartner, E., and Baltensperger, U.: Trace metals in ambient air:
34 Hourly size-segregated mass concentrations determined by synchrotron-XRF,
35 *Environ. Sci. Technol.*, 39, 5754-5762, 2005.

36 Bukowiecki, N., Lienemann, P., Zwicky, C. N., Furger, M., Richard, A., Falkenberg,
37 G., Rickers, K., Grolimund, D., Borca, C., Hill, M., Gehrig, R., and Baltensperger, U.:
38 X-ray fluorescence spectrometry for high throughput analysis of atmospheric aerosol
39 samples: The benefits of synchrotron X-rays, *Spectrochim. Acta B*, 63, 929-938,
40 2008.

41 Bukowiecki, N., Gehrig, R., Lienemann, P., Hill, M., Figi, R., Buchmann, B., Furger,
42 M., Richard, A., Mohr, C., Weimer, S., Prevot, A. S. H., and Baltensperger, U.: PM₁₀
43 emission factors of abrasion particles from road traffic, *Schweizerische*
44 *Eidgenossenschaft*, 2009a.

45 Bukowiecki, N., Lienemann, P., Hill, M., Figi, R., Richard, A., Furger, M., Rickers, K.,
46 Falkenberg, G., Zhao, Y. J., Cliff, S. S., Prevot, A. S. H., Baltensperger, U.,
47 Buchmann, B., and Gehrig, R.: Real-world emission factors for antimony and other
48 brake wear related trace elements: Size-segregated values for light and heavy duty
49 vehicles, *Environ. Sci. Technol.*, 43, 8072-8078, 2009b.

- 1 Bukowiecki, N., Richard, A., Furger, M., Weingartner, E., Aguirre, M., Huthwelker, T.,
2 Lienemann, P., Gehrig, R., and Baltensperger, U.: Deposition uniformity and particle
3 size distribution of ambient aerosol collected with a rotating drum impactor, *Aerosol*
4 *Sci. Technol.*, 43, 891-901, 2009c.
- 5 Bukowiecki, N., Lienemann, P., Hill, M., Furger, M., Richard, A., Amato, F., Prevot, A.
6 S. H., Baltensperger, U., Buchmann, B., and Gehrig, R.: PM10 emission factors for
7 non-exhaust particles generated by road traffic in an urban street canyon and along a
8 freeway in Switzerland, *Atmos. Env.*, 44, 2330-2340, 2010.
- 9 Calzolari, G., Chiari, M., Lucarelli, F., Nava, S., and Portarena, S.: Proton induced
10 gamma-ray emission yields for the analysis of light elements in aerosol samples in an
11 external beam set-up, *Nucl. Instrum. Methods Phys. Res. Sect. B-Beam Interact.*
12 *Mater. Atoms*, 268, 1540-1545, 2010.
- 13 Canonaco, F., Crippa, M., Slowik, J. G., Baltensperger, U., and Prevot, A. S. H.:
14 SoFi, an IGOR-based interface for the efficient use of the generalized multiline
15 engine (ME-2) for the source apportionment: ME-2 application to aerosol mass
16 spectrometer data, *Atmos. Meas. Tech.*, 6, 3649-3661, doi:10.5194/amt-6-3649-
17 2013, 2013.
- 18 Charron, A., and Harrison, R. M.: Fine (PM_{2.5}) and coarse (PM_{2.5-10}) particulate
19 matter on a heavily trafficked London highway: Sources and processes, *Environ. Sci.*
20 *Technol.*, 39, 7768-7776, doi:10.1021/es050462i, 2005.
- 21 Charron, A., Harrison, R. M., and Quincey, P.: What are the sources and conditions
22 responsible for exceedences of the 24 h PM₁₀ limit value (50 µg m⁻³) at a heavily
23 trafficked London site?, *Atmos. Env.*, 41, 1960-1975, 2007.
- 24 Crippa, M., DeCarlo, P. F., Slowik, J. G., Mohr, C., Heringa, M. F., Chirico, R.,
25 Poulain, L., Freutel, F., Sciare, J., Cozic, J., Di Marco, C. F., Elsasser, M., Nicolas, J.
26 B., Marchand, N., Abidi, E., Wiedensohler, A., Drewnick, F., Schneider, J., Borrmann,
27 S., Nemitz, E., Zimmermann, R., Jaffrezo, J. L., Prévôt, A. S. H., and Baltensperger,
28 U.: Wintertime aerosol chemical composition and source apportionment of the
29 organic fraction in the metropolitan area of Paris, *Atmos. Chem. Phys.*, 13, 961-981,
30 doi:10.5194/acp-13-961-2013, 2013.
- 31 DeCarlo, P. F., Kimmel, J. R., Trimborn, A., Northway, M. J., Jayne, J. T., Aiken, A.
32 C., Gonin, M., Fuhrer, K., Horvath, T., Docherty, K. S., Worsnop, D. R., and Jimenez,
33 J. L.: Field-deployable, high-resolution, time-of-flight aerosol mass spectrometer,
34 *Anal. Chem.*, 78, 8281-8289, doi:10.1021/ac061249n, 2006.
- 35 Dockery, D. W., and Pope, C. A., III: Acute respiratory effects of particulate air
36 pollution, in: *Annual Review of Public Health*, edited by: Omenn, G. S., *Annual*
37 *Review of Public Health*, Annual Reviews Inc., P.O. Box 10139, 4139 El Camino
38 Way, Palo Alto, California 94306, USA, 107-132, 1994.
- 39 Dore, C. J., Goodwin, J. W. L., Watterson, J. D., Murrels, T. P., Passant, N. R.,
40 Hobson, M. M., Haigh, K. E., Baggott, S. L., Pye, S. T., Coleman, P. J., and King, K.
41 R.: UK Emissions of Air Pollutants 1970 to 2001, *National Atmospheric Emissions*
42 *Inventory*, 2003.
- 43 Flechsig, U., Jaggi, A., Spielmann, S., Padmore, H. A., and MacDowell, A. A.: The
44 optics beamline at the Swiss Light Source, *Nucl. Instrum. Methods Phys. Res. Sect.*
45 *A-Accel. Spectrom. Dect. Assoc. Equip.*, 609, 281-285, 2009.
- 46 Formenti, P., Prati, P., Zucchiatti, A., Lucarelli, F., and Mando, P. A.: Aerosol study in
47 the town of Genova with a PIXE analysis, *Nucl. Instrum. Methods Phys. Res. Sect.*
48 *B-Beam Interact. Mater. Atoms*, 113, 359-362, 1996.

1 Formenti, P., Nava, S., Prati, P., Chevaillier, S., Klaver, A., Lafon, S., Mazzei, F.,
2 Calzolai, G., and Chiari, M.: Self-attenuation artifacts and correction factors of light
3 element measurements by X-ray analysis: Implication for mineral dust composition
4 studies, *J. Geophys. Res.-Atmos.*, 115, 8, doi:10.1029/2009jd012701, 2010.

5 Fowler, D., and Smith, R.: Spatial and temporal variability in the deposition of
6 acidifying species in the UK between 1986 and 1997, Department of Environment,
7 Food and Rural Affairs, 2000.

8 Franklin, M., Koutrakis, P., and Schwartz, J.: The role of particle composition on the
9 association between PM_{2.5} and mortality, *Epidemiology*, 19, 680-689,
10 doi:10.1097/ede.0b013e3181812bb7, 2008.

11 Freutel, F., Schneider, J., Drewnick, F., von der Weiden-Reinmüller, S. L., Crippa,
12 M., Prévôt, A. S. H., Baltensperger, U., Poulain, L., Wiedensohler, A., Sciare, J.,
13 Sarda-Estève, R., Burkhardt, J. F., Eckhardt, S., Stohl, A., Gros, V., Colomb, A.,
14 Michoud, V., Doussin, J. F., Borbon, A., Haeffelin, M., Morille, Y., Beekmann, M., and
15 Borrmann, S.: Aerosol particle measurements at three stationary sites in the
16 megacity of Paris during summer 2009: meteorology and air mass origin dominate
17 aerosol particle composition and size distribution, *Atmos. Chem. Phys.*, 13, 933-959,
18 doi:10.5194/acp-13-933-2013, 2013.

19 Gotschi, T., Hazenkamp-Von Arxb, M. E., Heinrich, J., Bono, R., Burney, P.,
20 Forsberg, B., Jarvis, D., Maldonado, J., Norback, D., Stern, W. B., Sunyer, J., Toren,
21 K., Verlato, G., Villani, S., and Kunzli, N.: Elemental composition and reflectance of
22 ambient fine particles at 21 European locations, *Atmos. Env.*, 39, 5947-5958, 2005.

23 Hammond, D. M., Dvonch, J. T., Keeler, G. J., Parker, E. A., Kamal, A. S., Barres, J.
24 A., Yip, F. Y., and Brakefield-Caldwell, W.: Sources of ambient fine particulate matter
25 at two community sites in Detroit, Michigan, *Atmos. Env.*, 42, 720-732, 2008.

26 Harrison, R. M., and Jones, A. M.: Multisite study of particle number concentrations
27 in urban air, *Environ. Sci. Technol.*, 39, 6063-6070, doi:10.1021/es040541e, 2005.

28 Harrison, R. M., Yin, J., Mark, D., Stedman, J., Appleby, R. S., Booker, J., and
29 Moorcroft, S.: Studies of the coarse particle (2.5–10 µm) component in UK urban
30 atmospheres, *Atmos. Env.*, 35, 3667-3679, 2001.

31 Harrison, R. M., Stedman, J., and Derwent, D.: New Directions: Why are PM₁₀
32 concentrations in Europe not falling?, *Atmos. Env.*, 42, 603-606, 2008.

33 Harrison, R. M., Beddows, D. C. S., and Dall'Osto, M.: PMF analysis of wide-range
34 particle size spectra collected on a major highway, *Environ. Sci. Technol.*, 45, 5522-
35 5528, 2011.

36 Harrison, R. M., Dall'Osto, M., Beddows, D. C. S., Thorpe, A. J., Bloss, W. J., Allan,
37 J. D., Coe, H., Dorsey, J. R., Gallagher, M., Martin, C., Whitehead, J., Williams, P. I.,
38 Jones, R. L., Langridge, J. M., Benton, A. K., Ball, S. M., Langford, B., Hewitt, C. N.,
39 Davison, B., Martin, D., Petersson, K. F., Henshaw, S. J., White, I. R., Shallcross, D.
40 E., Barlow, J. F., Dunbar, T., Davies, F., Nemitz, E., Phillips, G. J., Helfter, C., Di
41 Marco, C. F., and Smith, S.: Atmospheric chemistry and physics in the atmosphere of
42 a developed megacity (London): an overview of the REPARTEE experiment and its
43 conclusions, *Atmos. Chem. Phys.*, 12, 3065-3114, 2012a.

44 Harrison, R. M., Jones, A. M., Gietl, J., Yin, J., and Green, D. C.: Estimation of the
45 contributions of brake dust, tire wear, and resuspension to nonexhaust traffic
46 particles derived from atmospheric measurements, *Environ. Sci. Technol.*, 46, 6523-
47 6529, doi:10.1021/es300894r, 2012b.

- 1 Harrison, R. M., Laxen, D., Moorcroft, S., and Laxen, K.: Processes affecting
2 concentrations of fine particulate matter (PM_{2.5}) in the UK atmosphere, *Atmos. Env.*,
3 46, 115-124, 2012c.
- 4 Janssen, N. A. H., Van Mansom, D. F. M., Van Der Jagt, K., Harssema, H., and
5 Hoek, G.: Mass concentration and elemental composition of airborne particulate
6 matter at street and background locations, *Atmos. Env.*, 31, 1185-1193, 1997.
- 7 Jones, A. M., Harrison, R. M., and Baker, J.: The wind speed dependence of the
8 concentrations of airborne particulate matter and NO_x, *Atmos. Env.*, 44, 1682-1690,
9 2010.
- 10 Jones, A. R., Thomson, D. J., Hort, M., and Devenish, B.: The UK Met Office's next-
11 generation atmospheric dispersion model, NAME III, *Air Pollution Modeling and its*
12 *Application XVII*, edited by: Borrego, C., and Norman, A.-L., Springer, 2007.
- 13 Kelly, F. J., and Fussell, J. C.: Size, source and chemical composition as
14 determinants of toxicity attributable to ambient particulate matter, *Atmos. Env.*, 60,
15 504-526, 2012.
- 16 Lee, D. S., Garland, J. A., and Fox, A. A.: Atmospheric concentrations of trace
17 elements in urban areas of the United Kingdom, *Atmos. Env.*, 28, 2691-2713, 1994.
- 18 Lin, C. C., Chen, S. J., Huang, K. L., Hwang, W. I., Chang-Chien, G. P., and Lin, W.
19 Y.: Characteristics of metals in nano/ultrafine/fine/coarse particles collected beside a
20 heavily trafficked road, *Environ. Sci. Technol.*, 39, 8113-8122, 2005.
- 21 Lucarelli, F., Mando, P. A., Nava, S., Valerio, M., Prati, P., and Zucchiatti, A.:
22 Elemental composition of urban aerosol collected in Florence, Italy, *Environ. Monit.*
23 *Assess.*, 65, 165-173, 2000.
- 24 Maenhaut, W.: "Global Change" related and other atmospheric aerosol research at
25 the University of Gent, and the role of PIXE therein, *Nucl. Instrum. Methods Phys.*
26 *Res. Sect. B-Beam Interact. Mater. Atoms*, 109, 419-428, 1996.
- 27 Mavrogianni, A., Davies, M., Batty, M., Belcher, S. E., Bohnenstengel, S. I.,
28 Carruthers, D., Chalabi, Z., Croxford, B., Demanuele, C., Evans, S., Giridharan, R.,
29 Hacker, J. N., Hamilton, I., Hogg, C., Hunt, J., Kolokotroni, M., Martin, C., Milner, J.,
30 Rajapaksha, I., Ridley, I., Steadman, J. P., Stocker, J., Wilkinson, P., and Ye, Z.: The
31 comfort, energy and health implications of London's urban heat island, *Build Serv.*
32 *Eng. Res. Technol.*, 32, 35-52, doi:10.1177/0143624410394530, 2011.
- 33 Mazzei, F., Lucarelli, F., Nava, S., Prati, P., Valli, G., and Vecchi, R.: A new
34 methodological approach: The combined use of two-stage streaker samplers and
35 optical particle counters for the characterization of airborne particulate matter, *Atmos.*
36 *Env.*, 41, 5525-5535, 2007.
- 37 Minguillón, M. C., Cirach, M., Hoek, G., Brunekreef, B., Tsai, M., de Hoogh, K.,
38 Jedynska, A., Kooter, I. M., Nieuwenhuijsen, M., and Querol, X.: Spatial variability of
39 trace elements and sources for improved exposure assessment in Barcelona, *Atmos.*
40 *Env.*, 89, 268-281, 2014.
- 41 Moffet, R. C., Desyaterik, Y., Hopkins, R. J., Tivanski, A. V., Gilles, M. K., Wang, Y.,
42 Shutthanandan, V., Molina, L. T., Abraham, R. G., Johnson, K. S., Mugica, V.,
43 Molina, M. J., Laskin, A., and Prather, K. A.: Characterization of aerosols containing
44 Zn, Pb, and Cl from an industrial region of Mexico City, *Environ. Sci. Technol.*, 42,
45 7091-7097, 2008.
- 46 Mohr, C., Lopez-Hilfiker, F. D., Zotter, P., Prévôt, A. S. H., Xu, L., Ng, N. L., Herndon,
47 S. C., Williams, L. R., Franklin, J. P., Zahniser, M. S., Worsnop, D. R., Knighton, W.
48 B., Aiken, A. C., Gorkowski, K. J., Dubey, M. K., Allan, J. D., and Thornton, J. A.:
49 Contribution of nitrated phenols to wood burning brown carbon light absorption in

1 Detling, United Kingdom during winter time, *Environ. Sci. Technol.*, 47, 6316-6324,
2 doi:10.1021/es400683v, 2013.

3 Moreno, T., Karanasiou, A., Amato, F., Lucarelli, F., Nava, S., Calzolari, G., Chiari,
4 M., Coz, E., Artinano, B., Lumberras, J., Borge, R., Boldo, E., Linares, C., Alastuey,
5 A., Querol, X., and Gibbons, W.: Daily and hourly sourcing of metallic and mineral
6 dust in urban air contaminated by traffic and coal-burning emissions, *Atmos. Env.*,
7 68, 33-44, doi:10.1016/j.atmosenv.2012.11.037, 2013.

8 Nolte, C. G., Bhave, P. V., Arnold, J. R., Dennis, R. L., Zhang, K. M., and Wexler, A.
9 S.: Modeling urban and regional aerosols—Application of the CMAQ-UCD Aerosol
10 Model to Tampa, a coastal urban site, *Atmos. Env.*, 42, 3179-3191, 2008.

11 Paatero, P.: The multilinear engine—A table-driven, least squares program for
12 solving multilinear problems, including the n-way parallel factor analysis model, *J.*
13 *Comput. Graph. Stat.*, 8, 854-888, doi:10.1080/10618600.1999.10474853, 1999.

14 Putaud, J. P., Van Dingenen, R., Alastuey, A., Bauer, H., Birmili, W., Cyrus, J.,
15 Flentje, H., Fuzzi, S., Gehrig, R., Hansson, H. C., Harrison, R. M., Herrmann, H.,
16 Hitzenberger, R., Hüglin, C., Jones, A. M., Kasper-Giebl, A., Kiss, G., Kousa, A.,
17 Kuhlbusch, T. A. J., Löschau, G., Maenhaut, W., Molnar, A., Moreno, T., Pekkanen,
18 J., Perrino, C., Pitz, M., Puxbaum, H., Querol, X., Rodriguez, S., Salma, I., Schwarz,
19 J., Smolik, J., Schneider, J., Spindler, G., ten Brink, H., Tursic, J., Viana, M.,
20 Wiedensohler, A., and Raes, F.: A European aerosol phenomenology – 3: Physical
21 and chemical characteristics of particulate matter from 60 rural, urban, and kerbside
22 sites across Europe, *Atmos. Env.*, 44, 1308-1320, 2010.

23 Querol, X., Viana, M., Alastuey, A., Amato, F., Moreno, T., Castillo, S., Pey, J., de la
24 Rosa, J., Sánchez de la Campa, A., Artíñano, B., Salvador, P., García Dos Santos,
25 S., Fernández-Patier, R., Moreno-Grau, S., Negral, L., Minguillón, M. C., Monfort, E.,
26 Gil, J. I., Inza, A., Ortega, L. A., Santamaría, J. M., and Zabalza, J.: Source origin of
27 trace elements in PM from regional background, urban and industrial sites of Spain,
28 *Atmos. Env.*, 41, 7219-7231, 2007.

29 Reche, C., Moreno, T., Amato, F., Viana, M., van Drooge, B. L., Chuang, H.-C.,
30 Bérubé, K., Jones, T., Alastuey, A., and Querol, X.: A multidisciplinary approach to
31 characterise exposure risk and toxicological effects of PM10 and PM2.5 samples in
32 urban environments, *Ecotox. Environ. Safe.*, 78, 327-335, 2012.

33 Richard, A., Bukowiecki, N., Lienemann, P., Furger, M., Fierz, M., Minguillon, M. C.,
34 Weideli, B., Figi, R., Flechsig, U., Appel, K., Prevot, A. S. H., and Baltensperger, U.:
35 Quantitative sampling and analysis of trace elements in atmospheric aerosols:
36 impactor characterization and synchrotron-XRF mass calibration, *Atmos. Meas.*
37 *Tech.*, 3, 1473-1485, 2010.

38 Richard, A., Gianini, M. F. D., Mohr, C., Furger, M., Bukowiecki, N., Minguillon, M. C.,
39 Lienemann, P., Flechsig, U., Appel, K., DeCarlo, P. F., Heringa, M. F., Chirico, R.,
40 Baltensperger, U., and Prevot, A. S. H.: Source apportionment of size and time
41 resolved trace elements and organic aerosols from an urban courtyard site in
42 Switzerland, *Atmos. Chem. Phys.*, 11, 8945-8963, 2011.

43 Salcedo, D., Laskin, A., Shutthanandan, V., and Jimenez, J. L.: Feasibility of the
44 detection of trace elements in particulate matter using online high-resolution aerosol
45 mass spectrometry, *Aerosol Sci. Technol.*, 46, 1187-1200,
46 doi:10.1080/02786826.2012.701354, 2012.

47 Theodosi, C., Grivas, G., Zarpas, P., Chaloulakou, A., and Mihalopoulos, N.: Mass
48 and chemical composition of size-segregated aerosols (PM1, PM2.5, PM10) over
49 Athens, Greece: local versus regional sources, *Atmos. Chem. Phys.*, 11, 11895-
50 11911, doi:10.5194/acp-11-11895-2011, 2011.

- 1 Turoczi, B., Hoffer, A., Toth, A., Kovats, N., Acs, A., Ferincz, A., Kovacs, A., and
2 Gelencser, A.: Comparative assessment of ecotoxicity of urban aerosol, *Atmos.*
3 *Chem. Phys.*, 12, 7365-7370, doi:10.5194/acp-12-7365-2012, 2012.
- 4 Viana, M., Kuhlbusch, T. A. J., Querol, X., Alastuey, A., Harrison, R. M., Hopke, P.
5 K., Winiwarter, W., Vallius, A., Szidat, S., Prevot, A. S. H., Hueglin, C., Bloemen, H.,
6 Wahlin, P., Vecchi, R., Miranda, A. I., Kasper-Giebl, A., Maenhaut, W., and
7 Hitzenberger, R.: Source apportionment of particulate matter in Europe: A review of
8 methods and results, *J. Aerosol Sci.*, 39, 827-849,
9 doi:10.1016/j.jaerosci.2008.05.007, 2008.
- 10 Wedepohl, K.: The composition of the continental crust, *Geochim. Cosmochim. Ac.*,
11 59, 1217-1232, doi:10.1016/0016-7037(95)00038-2, 1995.
- 12 Weijers, E. P., Schaap, M., Nguyen, L., Matthijsen, J., van der Gon, H., ten Brink, H.
13 M., and Hoogerbrugge, R.: Anthropogenic and natural constituents in particulate
14 matter in the Netherlands, *Atmos. Chem. Phys.*, 11, 2281-2294, doi:10.5194/acp-11-
15 2281-2011, 2011.
- 16 Witt, M. L. I., Meheran, N., Mather, T. A., de Hoog, J. C. M., and Pyle, D. M.: Aerosol
17 trace metals, particle morphology and total gaseous mercury in the atmosphere of
18 Oxford, UK, *Atmos. Env.*, 44, 1524-1538, doi:10.1016/j.atmosenv.2010.01.008, 2010.
- 19 Wood, C. R., Lacser, A., Barlow, J. F., Padhra, A., Belcher, S. E., Nemitz, E., Helfter,
20 C., Famulari, D., and Grimmond, C. S. B.: Turbulent flow at 190 m height above
21 London during 2006-2008: A climatology and the applicability of similarity theory,
22 *Bound.-Layer Meteor.*, 137, 77-96, doi:10.1007/s10546-010-9516-x, 2010.
- 23 Xiao, Z. H., Shao, L. Y., Zhang, N., Wang, J., and Wang, J. Y.: Heavy metal
24 compositions and bioreactivity of airborne PM₁₀ in a valley-shaped city in
25 northwestern China, *Aerosol Air Qual. Res.*, 13, 1116-1125,
26 doi:10.4209/aaqr.2012.10.0287, 2013.
- 27 Zhou, J. A., Ito, K., Lall, R., Lippmann, M., and Thurston, G.: Time-series analysis of
28 mortality effects of fine particulate matter components in Detroit and Seattle, *Environ.*
29 *Health Perspect.*, 119, 461-466, doi:10.1289/ehp.1002613, 2011.
- 30 Zhou, Y., and Levy, J. I.: The impact of urban street canyons on population exposure
31 to traffic-related primary pollutants, *Atmos. Env.*, 42, 3087-3098, 2008.
- 32

1 **Tables**

2

3 **Table 1.** Measurement campaign details.

Site	Start/End date	Site type	Sampling time	Inlet height	Sampling platform
MR	11 Jan – 14 Feb 2012	kerbside	2 h	4 m	container at 1 m from road
NK	11 Jan – 9 Feb 2012	urban background	2 h	4 m	container
DE	17 Jan – 13 Feb 2012	rural	2 h	1.5 m	grass field

4

5

1 **Table 2.** Self-absorption correction factors.

Particle size (μm) ^a	Calibration standard 1		Calibration standard 2		PM _{10-2.5} sample		PM _{2.5-1.0} sample		Total correction factor ^d		
	AF ^c	a^c	AF ^c	a^c	AF ^c	a^c	AF ^c	a^c	PM _{10-2.5} sample	PM _{2.5-1.0} sample	PM _{1.0-0.3} sample
Density (g cm ⁻³) ^b	2.19		2.27		2.00		2.00				
Na	0.22	0.49			0.43	0.40	0.74	0.40	0.52	0.30	0.22
Mg			0.32	0.33	0.58	0.25	0.83	0.25	0.55	0.38	0.32
Al	0.43	0.23			0.70	0.15	0.89	0.15	0.61	0.48	0.43
Si			0.51	0.17	0.79	0.10	0.93	0.10	0.64	0.55	0.51
P	0.60	0.13			0.85	0.07	0.95	0.07	0.70	0.63	0.60
S			0.65	0.10	0.90	0.04	0.97	0.04	0.72	0.67	0.65
Cl	0.71	0.08			0.88	0.05	0.96	0.05	0.80	0.73	0.71
K			0.79	0.05	0.94	0.03	0.98	0.03	0.84	0.81	0.79
Ca	0.82	0.05	0.76	0.06	0.95	0.02	0.98	0.02	0.87 ^e	0.84 ^e	0.82 ^e

2 ^a Particle size given as geometric mean diameter.

3 ^b Average density of the calibration standards and of ambient aerosol. The composition of
 4 calibration standard 1 is Na_{3.76}Al_{3.76}P_{3.76}Cl_{3.76}Ca_{3.76}CoN₈O₂₄, of calibration standard 2
 5 Mg_{3.76}Si_{3.76}S_{3.76}K_{3.76}Ca_{3.76}CoN₇O₂₁, and of ambient samples C₃₉H₂₉N₁₀O₁₈S₃Fe.

6 ^c Attenuation factors and a (μm^{-1} ; $a = 2/3 * \mu * \rho$ with μ the mass attenuation coefficient ($\text{cm}^2 \text{g}^{-1}$)
 7 and ρ the particle mass density (g cm^{-3})) according to Eq. (4) in Formenti et al. (2010).

8 ^d Total correction factor defined as ratios AF calibration standard / AF sample. Self-absorption
 9 effects are neglected in the PM_{1.0-0.3} samples; therefore these samples are only corrected for
 10 AF calibration standards.

11 ^e Ca is corrected based on the average AF of calibration standards 1 and 2, and a calibration
 12 standard used to calibrate the elements Ti to Zn at SLS (Ca present in all three standards).
 13 Data for this third calibration standard are: particle size of $7.0 \pm 2 \mu\text{m}$, average density of 2.37
 14 g cm^{-3} and AF and a for Ca of 0.89 and $0.03 \mu\text{m}^{-1}$, respectively.

15
 16

1 **Table 3.** Mean, median and 25-75th percentile trace element concentrations (ng m⁻³)
 2 for PM_{10-2.5}, PM_{2.5-1.0} and PM_{1.0-0.3} at MR, NK and DE.

Marylebone Road												
Element	PM _{10-2.5}				PM _{2.5-1.0}				PM _{1.0-0.3}			
	mean	median	25th perc	75th perc	mean	median	25th perc	75th perc	mean	median	25th perc	75th perc
Na	913.7	854.2	447.9	1301.6	121.6	85.2	53.6	159.1	27.5	15.9	10.7	28.0
Mg	104.5	95.6	65.6	135.4	25.3	19.6	13.5	34.3	8.3	7.0	4.9	9.6
Al	82.4	66.5	44.9	102.7	23.1	20.7	15.4	28.3	5.8	5.4	3.6	7.2
Si	190.0	147.0	89.9	244.3	54.8	43.7	25.3	70.7	14.9	12.3	7.4	19.0
P	11.4	10.1	6.9	14.6	4.2	3.8	2.4	5.6	2.9	2.2	1.5	3.9
S	90.2	80.0	56.8	111.3	43.1	36.0	25.7	54.4	127.1	53.8	24.3	185.2
Cl	790.6	689.4	292.7	1164.4	217.4	110.0	30.6	329.1	81.2	25.2	5.1	103.4
K	36.2	32.4	23.1	44.0	13.1	11.3	7.6	17.4	14.1	9.4	6.3	18.4
Ca	201.9	152.4	93.6	265.6	62.0	43.9	26.7	79.3	16.7	12.3	7.4	20.7
Ti	7.5	5.9	3.4	10.0	2.6	2.0	1.2	3.6	0.8	0.7	0.4	1.1
V	2.2	1.9	1.1	2.9	0.9	0.8	0.4	1.1	0.4	0.4	0.2	0.6
Cr	6.3	3.6	2.0	6.0	1.7	1.4	0.9	2.4	0.6	0.4	0.3	0.7
Mn	9.4	7.7	4.6	12.2	3.4	2.9	2.0	4.4	1.4	1.0	0.6	1.7
Fe	693.1	601.7	347.0	929.9	259.9	226.8	136.4	348.6	90.4	75.8	43.6	122.3
Ni	2.1	0.6	0.4	1.0	0.3	0.2	0.1	0.4	0.2	0.1	0.1	0.2
Cu	26.0	22.9	12.6	33.3	9.5	8.2	4.6	12.5	3.3	2.6	1.4	4.5
Zn	10.9	8.9	5.2	14.1	4.3	3.6	2.0	5.6	4.6	3.0	1.6	6.5
Br	2.3	1.8	1.0	3.0	0.8	0.6	0.4	1.0	1.7	1.1	0.6	2.3
Sr	1.1	0.9	0.7	1.4	0.4	0.4	0.2	0.6	0.2	0.1	0.1	0.2
Zr	2.5	1.8	0.9	3.3	1.1	0.8	0.4	1.4	0.4	0.2	0.1	0.5
Mo	3.1	2.2	1.1	3.9	1.3	1.0	0.6	1.6	0.5	0.4	0.2	0.6
Sn	4.1	3.3	1.9	5.5	1.7	1.5	0.8	2.3	0.7	0.6	0.3	1.0
Sb	3.3	2.5	1.3	4.4	1.3	1.0	0.6	1.8	0.5	0.4	0.3	0.7
Ba	18.3	14.5	8.3	24.7	7.6	6.5	3.9	10.3	2.7	2.1	1.2	3.7
Pb	1.6	0.9	0.6	1.7	0.7	0.5	0.3	0.9	1.6	0.8	0.4	2.1

North Kensington												
Element	PM _{10-2.5}				PM _{2.5-1.0}				PM _{1.0-0.3}			
	mean	median	25th perc	75th perc	mean	median	25th perc	75th perc	mean	median	25th perc	75th perc
Na	595.1	511.6	269.6	897.9	123.5	87.1	56.4	163.7	28.6	14.2	9.8	31.7
Mg	57.2	49.9	30.2	83.9	23.0	17.9	12.7	30.8	7.1	5.2	3.1	8.8
Al	30.8	26.0	16.3	40.8	17.1	15.5	10.2	20.7	4.4	3.8	2.7	5.4
Si	63.1	51.2	25.6	78.7	33.1	26.5	14.7	45.0	8.3	5.9	3.5	10.2
P	4.5	4.0	2.3	6.3	2.7	2.3	1.4	3.3	1.9	1.4	0.8	2.4
S	45.8	40.7	27.5	61.7	36.1	28.8	20.3	44.2	113.3	53.1	24.6	137.0
Cl	435.6	343.1	110.6	702.3	199.2	79.1	18.2	289.8	63.7	9.9	2.5	66.6
K	18.9	16.7	10.8	25.9	11.5	9.9	6.7	16.1	12.2	8.1	4.9	14.8
Ca	79.9	60.7	35.0	99.0	41.7	31.1	17.5	50.1	9.7	7.1	4.0	11.6
Ti	2.7	1.7	0.9	3.2	1.6	1.2	0.5	2.3	0.4	0.3	0.1	0.5
V	0.6	0.4	0.2	0.7	0.4	0.3	0.1	0.5	0.2	0.2	0.1	0.3
Cr	1.2	0.8	0.4	1.5	0.6	0.5	0.3	0.8	0.2	0.1	0.0	0.2
Mn	2.4	1.7	1.0	3.0	1.7	1.5	0.8	2.2	0.8	0.5	0.1	0.9
Fe	163.8	120.8	69.9	202.6	98.8	72.7	39.0	126.0	30.1	18.5	9.6	34.8
Ni	0.4	0.2	0.1	0.4	0.1	0.1	0.0	0.2	0.1	0.1	0.0	0.1
Cu	4.9	3.6	1.8	6.4	3.7	2.5	1.4	4.6	1.2	0.6	0.4	1.4
Zn	2.9	1.9	1.0	3.4	2.1	1.5	0.8	2.8	3.2	1.9	0.8	4.3
Br	1.3	1.0	0.4	1.8	0.7	0.5	0.3	1.0	1.6	1.1	0.5	1.9
Sr	0.5	0.4	0.2	0.6	0.3	0.2	0.2	0.4	0.1	0.1	0.0	0.1
Zr	0.5	0.2	0.1	0.4	0.3	0.2	0.1	0.4	0.1	0.1	0.0	0.1
Mo	0.8	0.3	0.2	0.7	0.5	0.3	0.1	0.6	0.2	0.1	0.1	0.2
Sn	0.7	0.5	0.2	0.9	0.5	0.4	0.2	0.7	0.3	0.2	0.1	0.3
Sb	0.5	0.3	0.2	0.6	0.4	0.2	0.1	0.5	0.2	0.2	0.1	0.3
Ba	4.3	2.1	1.2	4.5	2.7	1.8	0.9	3.5	1.0	0.6	0.3	1.2
Pb	0.4	0.2	0.1	0.4	0.4	0.2	0.1	0.6	1.4	0.7	0.3	1.8

Detling Element	PM _{10-2.5}				PM _{2.5-1.0}				PM _{1.0-0.3}			
	mean	median	25th perc	75th perc	mean	median	25th perc	75th perc	mean	median	25th perc	75th perc
Na	271.9	194.7	17.2	437.0	66.2	37.2	13.0	82.2	21.3	11.4	5.0	28.3
Mg	27.5	20.8	5.2	39.9	12.4	8.8	2.7	17.1	6.2	4.4	1.6	7.7
Al	15.6	14.4	7.4	21.5	13.4	12.9	6.7	18.4	3.2	3.1	1.5	4.7
Si	32.5	26.3	13.8	41.5	17.3	13.7	6.1	25.3	5.5	4.3	2.4	7.9
P	2.2	1.8	0.8	2.9	1.3	1.0	0.5	1.7	1.9	1.0	0.5	2.4
S	26.1	22.8	4.9	34.6	22.3	20.4	8.8	32.1	145.2	38.8	18.0	157.4
Cl	189.6	40.5	2.9	303.7	99.1	6.8	1.9	109.0	45.4	7.3	2.4	40.4
K	11.7	10.0	2.9	14.9	6.6	6.1	2.1	10.1	15.7	6.4	2.9	15.6
Ca	32.5	24.9	9.6	40.3	16.7	12.3	4.9	21.0	6.7	4.1	2.2	6.8
Ti	1.0	0.6	0.3	1.3	0.7	0.4	0.2	1.0	0.2	0.2	0.1	0.3
V	0.2	0.1	0.1	0.2	0.1	0.1	0.1	0.2	0.2	0.1	0.0	0.3
Cr	4.0	0.9	0.3	2.9	0.8	0.3	0.2	0.6	0.1	0.1	0.0	0.2
Mn	1.8	0.6	0.3	1.3	1.1	1.2	0.3	1.6	0.7	0.3	0.0	0.7
Fe	55.2	36.8	19.9	66.2	26.8	21.5	11.5	37.7	9.8	7.8	4.3	13.3
Ni	4.3	0.7	0.2	2.6	0.6	0.1	0.1	0.3	0.9	0.1	0.0	0.5
Cu	1.4	0.8	0.4	1.8	0.9	0.7	0.4	1.1	0.7	0.3	0.1	0.5
Zn	3.4	0.9	0.4	1.8	1.3	0.7	0.3	1.7	4.3	1.6	0.6	5.7
Br	1.1	0.4	0.1	1.3	0.4	0.2	0.1	0.5	1.9	1.1	0.5	2.4
Sr	0.2	0.2	0.1	0.3	0.1	0.1	0.0	0.2	0.1	0.0	0.0	0.1
Zr	0.0	0.0	-0.1	0.1	0.1	0.0	0.0	0.1	0.0	0.0	0.0	0.0
Mo	1.9	0.1	0.1	0.7	0.2	0.1	0.0	0.2	0.1	0.1	0.0	0.1
Sn	0.3	0.1	0.0	0.2	0.2	0.1	0.1	0.2	0.2	0.1	0.1	0.3
Sb	0.2	0.1	0.0	0.2	0.1	0.1	0.0	0.1	0.2	0.1	0.0	0.2
Ba	1.0	0.4	0.2	0.8	0.5	0.4	0.2	0.7	0.3	0.2	0.1	0.4
Pb	0.3	0.1	0.0	0.3	0.3	0.1	0.1	0.5	1.6	0.5	0.2	1.8

1

2

1 **Figure captions**

2

3 **Figure 1.** Map of south eastern UK. Indicated are the sampling sites MR (kerbside
4 site Marylebone Road), NK (urban background site North Kensington), DE (rural site
5 Detling), and the elevated BT Tower site for meteorological measurements (adapted
6 from Google Maps).

7

8 **Figure 2.** Relative contribution for trace elements in $PM_{10-2.5}$, $PM_{2.5-1.0}$ and $PM_{1.0-0.3}$ to
9 total PM_{10} mean concentration per element at MR (top), NK (middle) and DE
10 (bottom). Absolute mean total PM_{10} element concentrations are shown above each
11 bar.

12

13 **Figure 3.** Mean, median and 25-75th percentile urban increment values for trace
14 elements at NK relative to DE for $PM_{10-2.5}$ (top), $PM_{2.5-1.0}$ (middle) and $PM_{1.0-0.3}$
15 (bottom). Note that the median of Zr in $PM_{10-2.5}$ is below detection limit.

16

17 **Figure 4.** Mean, median and 25-75th percentile trace element concentrations at MR
18 split in four wind direction sectors (N, E, S, W) normalized to the global median
19 concentration per element for $PM_{10-2.5}$ (top), $PM_{2.5-1.0}$ (middle) and $PM_{1.0-0.3}$ (bottom).
20 See Sect. 4.2.2 for the definition of the wind direction sectors.

21

22 **Figure 5.** Mean, median and 25-75th percentile kerb increment values for trace
23 elements at MR relative to NK for $PM_{10-2.5}$ (top), $PM_{2.5-1.0}$ (middle) and $PM_{1.0-0.3}$
24 (bottom) split in SW and NE wind sectors. See Sect. 4.2.2 for the definition of the
25 wind direction sectors.

26

27 **Figure 6.** Diurnal cycles of 2 h median concentrations of Na, Si, S, Fe and Sb for
28 $PM_{10-2.5}$ (left), $PM_{2.5-1.0}$ (middle) and $PM_{1.0-0.3}$ (right) at MR, NK, DE split in SW and NE
29 wind sectors. See Sect. 4.2.2 for the definition of the wind direction sectors. Hour of
30 day is start of 2 h sampling period, so 00:00 LT means sampling from 00:00 to 02:00
31 LT.

32

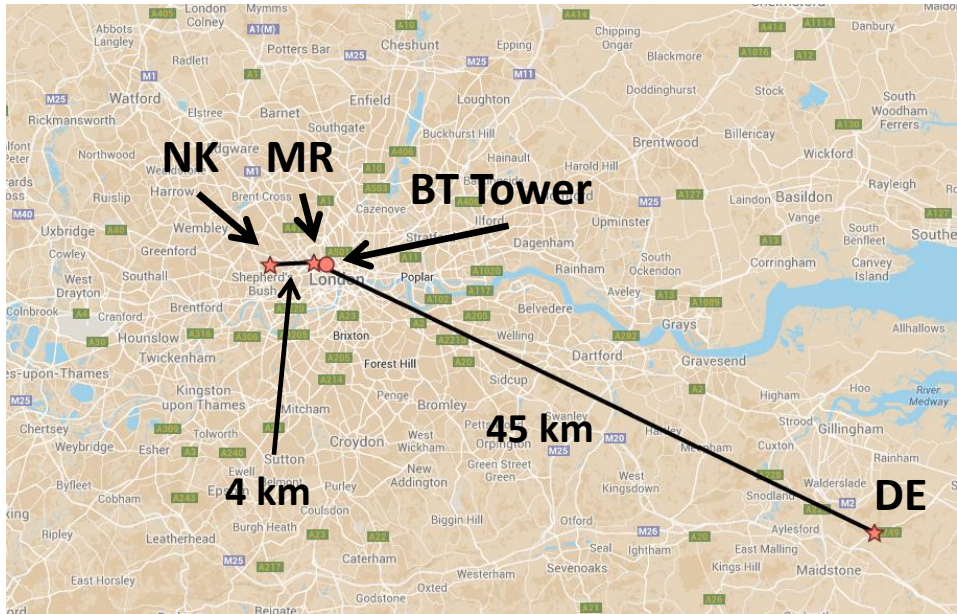
33 **Figure 7.** Weekly cycles of 2 h median concentrations of Na, Si, S, Fe and Sb for
34 $PM_{10-2.5}$ (left), $PM_{2.5-1.0}$ (middle) and $PM_{1.0-0.3}$ (right) at MR, NK, DE.

35

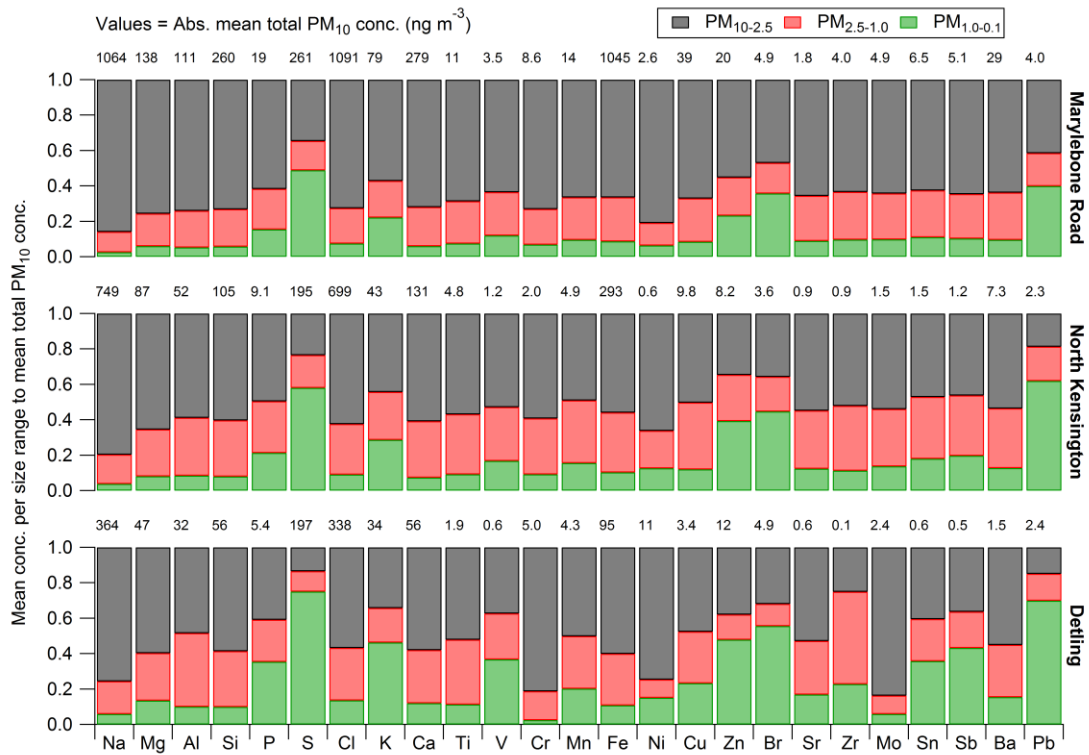
1 **Figure 8.** (top) Diurnal (left) and weekly (right) cycles of traffic flow at MR, (middle
2 and bottom left) diurnal cycles of 2 h median NO_x and total PM_{10} mass
3 concentrations at MR, NK and DE split in SW and NE wind sectors, and (middle and
4 bottom right) weekly cycles of 2 h median NO_x and total PM_{10} mass concentrations at
5 MR, NK and DE. See Sect. 4.2.2 for the definition of the wind direction sectors. Time
6 stamp is start of 2 h averaging period, so 00:00 LT means averaging between 00:00
7 and 02:00 LT.

8
9 **Figure 9.** (top panel) Time series of (top left axis) $\text{PM}_{1.0-0.3}$ S, K, Zn and Pb
10 concentrations at NK and (top right axis) wind direction from BT Tower, time series of
11 (bottom left axis) $\text{PM}_{10-2.5}$ Na, Si, S and Sb concentrations at NK and (bottom right
12 axis) total PM_{10} mass concentration at NK; (bottom panel) three NK footprints
13 simulated with the NAME model corresponding to the vertical lines (A, B, C) indicated
14 in the top panel. Trajectories are simulated for particles released from NK and
15 followed back at 0-100 m a.g.l. for the previous 24 h at: **(A)** 23 January 2012 09:00
16 LT, **(B)** 31 January 2012 21:00 LT, **(C)** 6 February 2012 18:00 LT; particle
17 concentrations increase from blue to red.

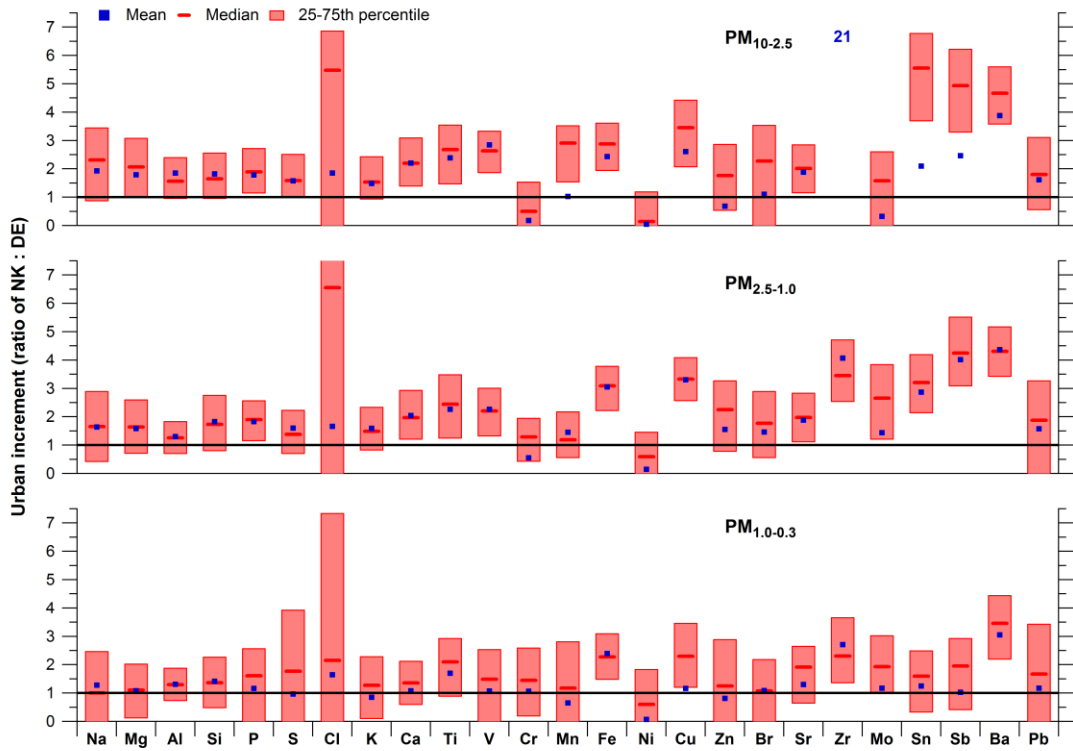
18
19



1
2 **Figure 1.** Map of south eastern UK. Indicated are the sampling sites MR (kerbside
3 site Marylebone Road), NK (urban background site North Kensington), DE (rural site
4 Detling), and the elevated BT Tower site for meteorological measurements (adapted
5 from Google Maps).
6

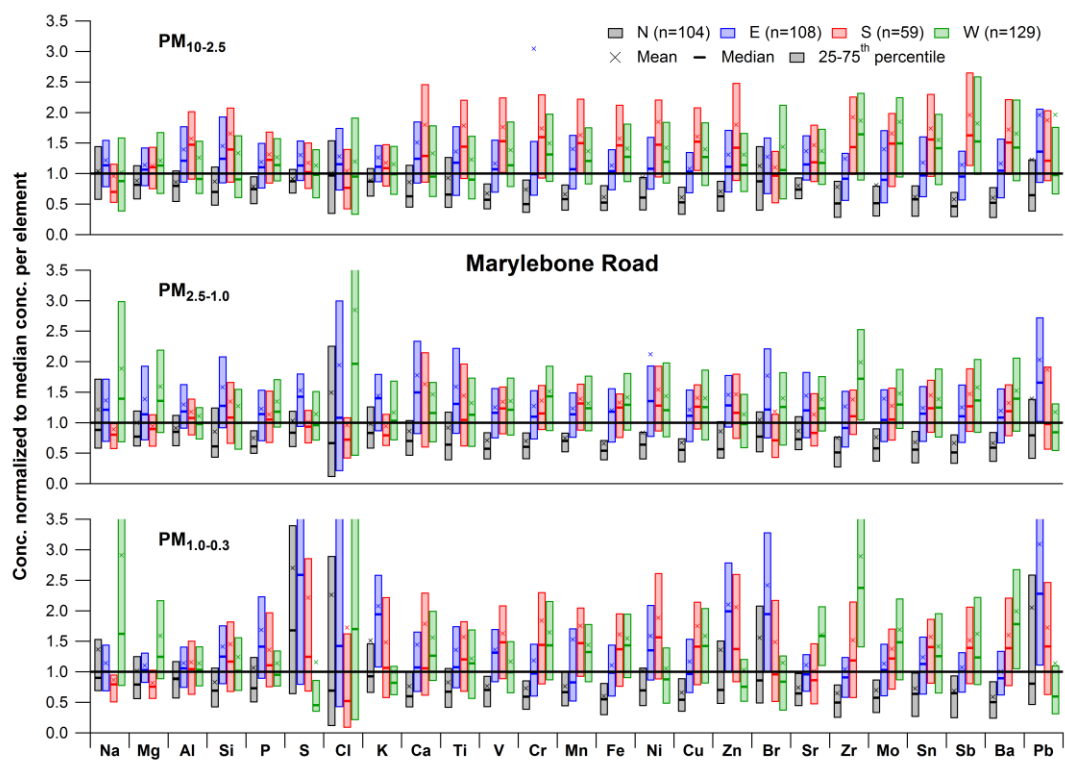


1
 2 **Figure 2.** Relative contribution for trace elements in PM_{10-2.5}, PM_{2.5-1.0} and PM_{1.0-0.3} to
 3 total PM₁₀ mean concentration per element at MR (top), NK (middle) and DE
 4 (bottom). Absolute mean total PM₁₀ element concentrations are shown above each
 5 bar.
 6

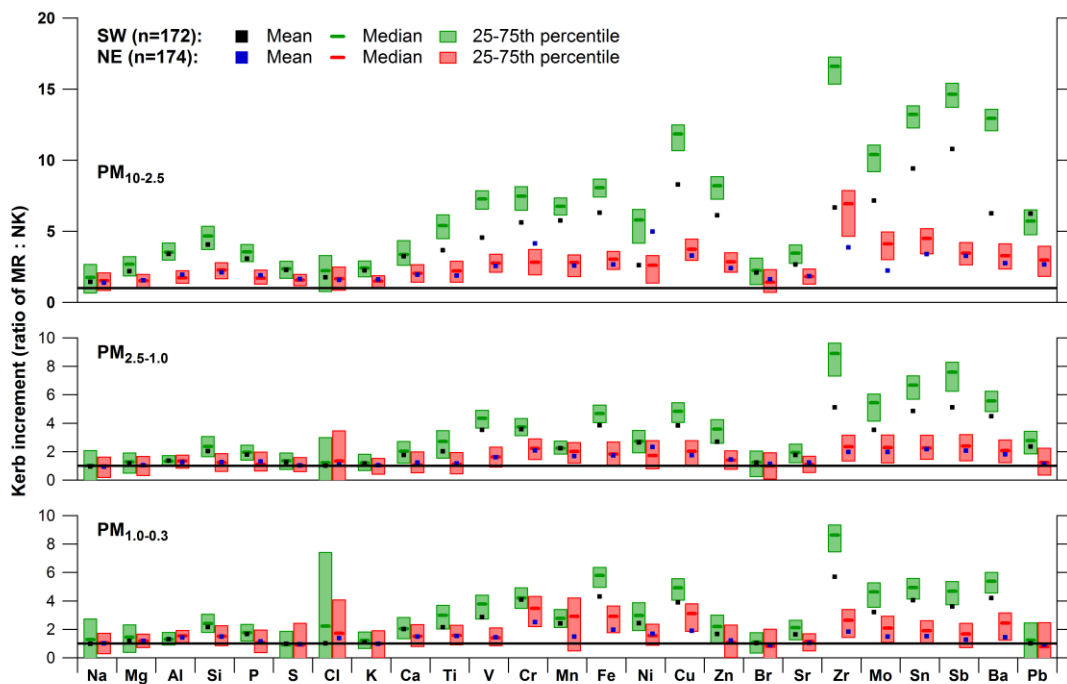


1
2
3
4
5

Figure 3. Mean, median and 25-75th percentile urban increment values for trace elements at NK relative to DE for $PM_{10-2.5}$ (top), $PM_{2.5-1.0}$ (middle) and $PM_{1.0-0.3}$ (bottom). Note that the median of Zr in $PM_{10-2.5}$ is below detection limit.

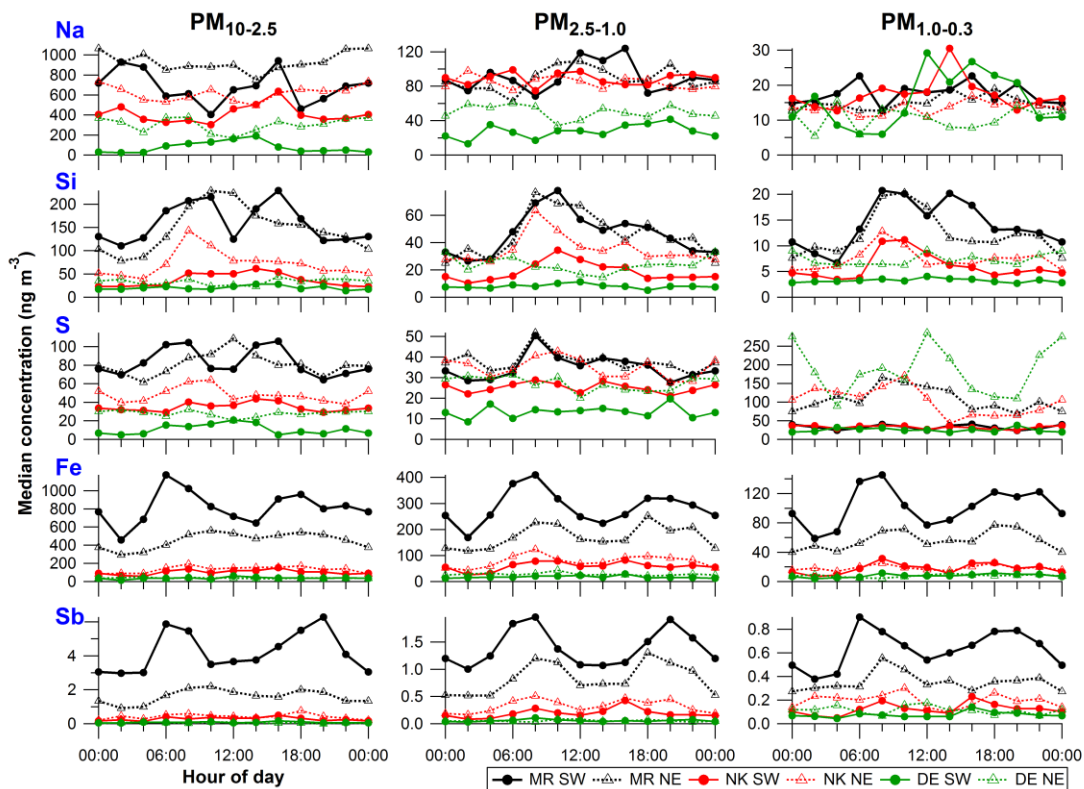


1
 2 **Figure 4.** Mean, median and 25-75th percentile trace element concentrations at MR
 3 split in four wind direction sectors (N, E, S, W) normalized to the global median
 4 concentration per element for $PM_{10-2.5}$ (top), $PM_{2.5-1.0}$ (middle) and $PM_{1.0-0.3}$ (bottom).
 5 See Sect. 4.2.2 for the definition of the wind direction sectors.
 6



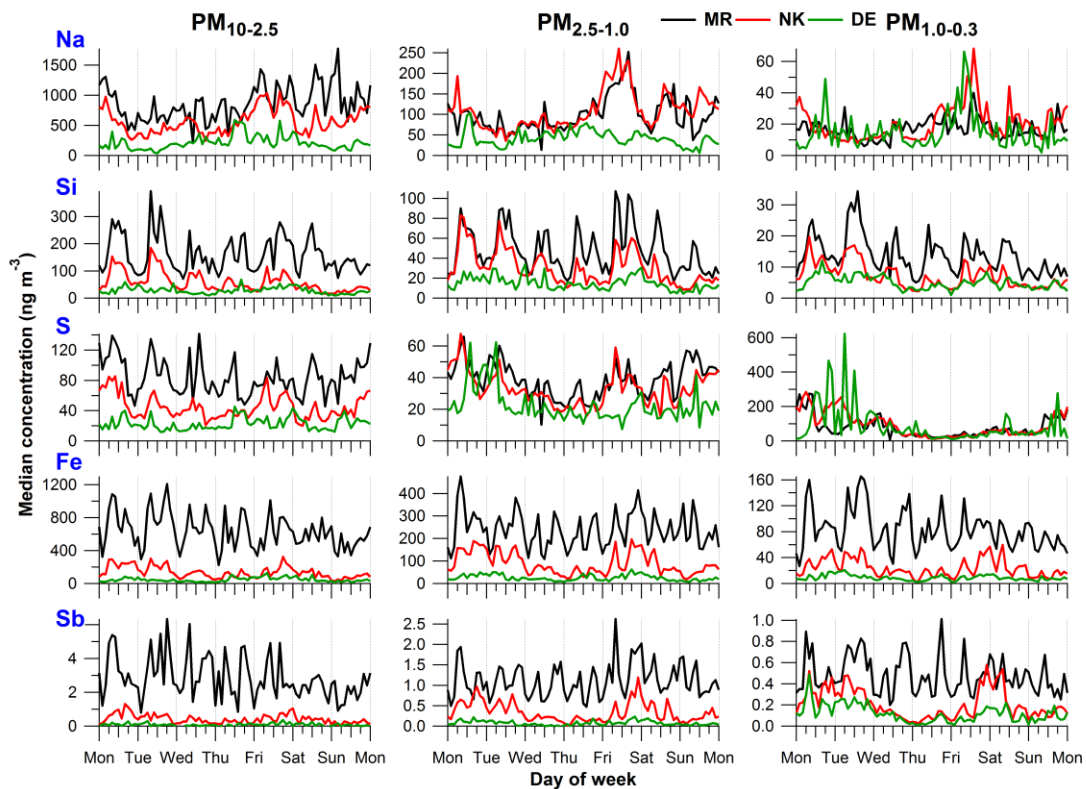
1
2
3
4
5
6

Figure 5. Mean, median and 25-75th percentile kerb increment values for trace elements at MR relative to NK for $PM_{10-2.5}$ (top), $PM_{2.5-1.0}$ (middle) and $PM_{1.0-0.3}$ (bottom) split in SW and NE wind sectors. See Sect. 4.2.2 for the definition of the wind direction sectors.



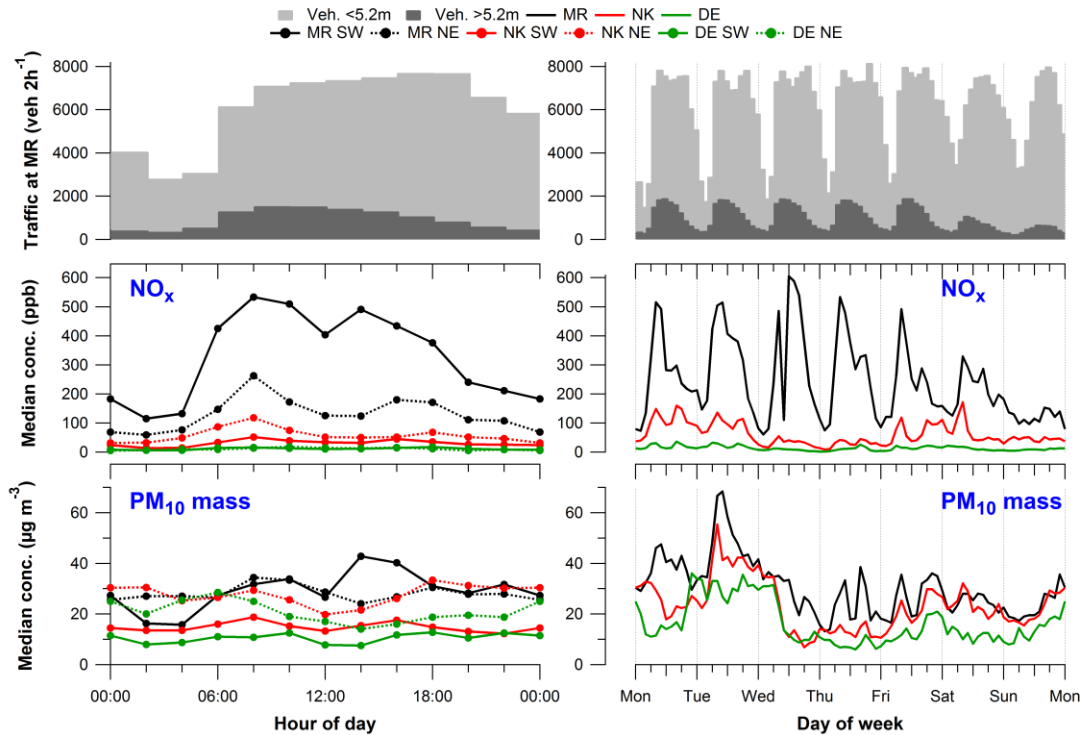
1
2
3
4
5
6
7

Figure 6. Diurnal cycles of 2 h median concentrations of Na, Si, S, Fe and Sb for PM_{10-2.5} (left), PM_{2.5-1.0} (middle) and PM_{1.0-0.3} (right) at MR, NK, DE split in SW and NE wind sectors. See Sect. 4.2.2 for the definition of the wind direction sectors. Hour of day is start of 2 h sampling period, so 00:00 LT means sampling from 00:00 to 02:00 LT.

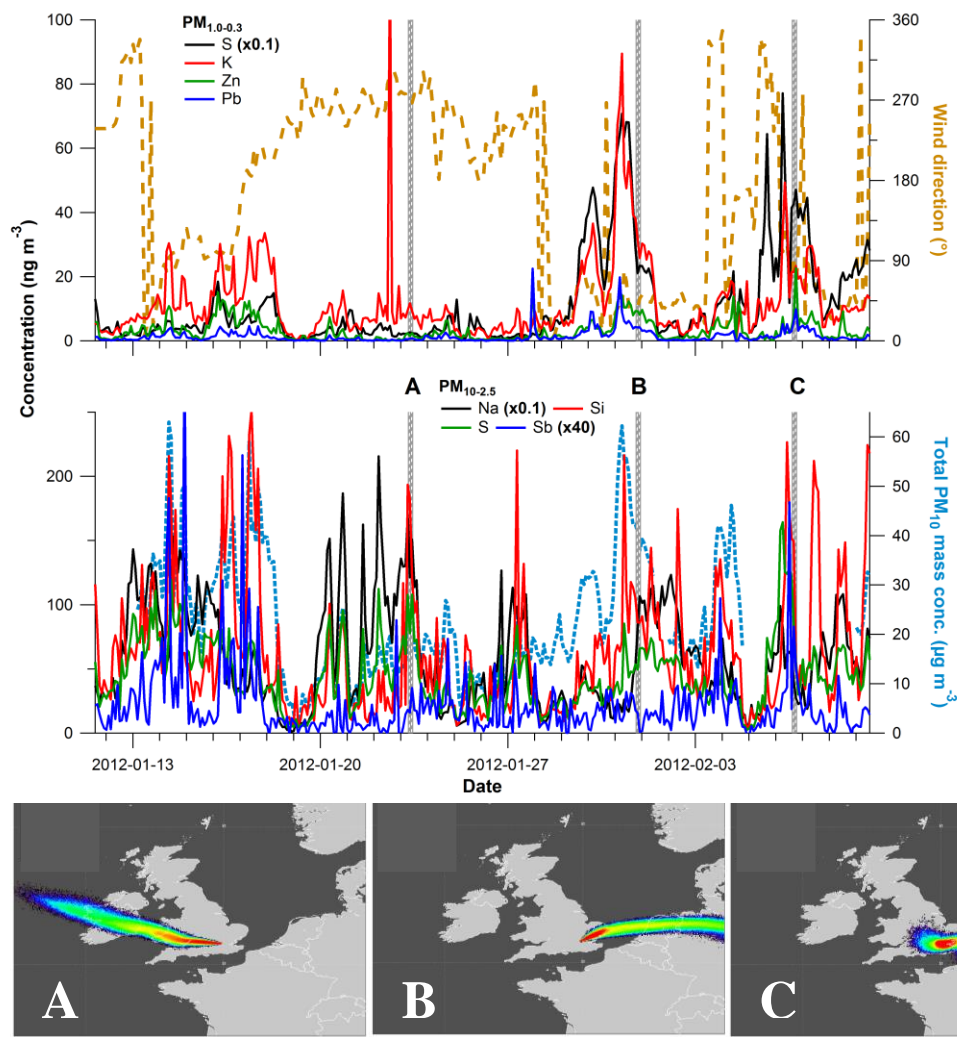


1
2
3
4

Figure 7. Weekly cycles of 2 h median concentrations of Na, Si, S, Fe and Sb for PM_{10-2.5} (left), PM_{2.5-1.0} (middle) and PM_{1.0-0.3} (right) at MR, NK, DE.



1
 2 **Figure 8.** (top) Diurnal (left) and weekly (right) cycles of traffic flow at MR, (middle
 3 and bottom left) diurnal cycles of 2 h median NO_x and total PM₁₀ mass
 4 concentrations at MR, NK and DE split in SW and NE wind sectors, and (middle and
 5 bottom right) weekly cycles of 2 h median NO_x and total PM₁₀ mass concentrations at
 6 MR, NK and DE. See Sect. 4.2.2 for the definition of the wind direction sectors. Time
 7 stamp is start of 2 h averaging period, so 00:00 LT means averaging between 00:00
 8 and 02:00 LT.
 9



1
2 **Figure 9.** (top panel) Time series of (top left axis) $PM_{1.0-0.3}$ S, K, Zn and Pb
3 concentrations at NK and (top right axis) wind direction from BT Tower, time series of
4 (bottom left axis) $PM_{10-2.5}$ Na, Si, S and Sb concentrations at NK and (bottom right
5 axis) total PM_{10} mass concentration at NK; (bottom panel) three NK footprints
6 simulated with the NAME model corresponding to the vertical lines (A, B, C) indicated
7 in the top panel. Trajectories are simulated for particles released from NK and
8 followed back at 0-100 m a.g.l. for the previous 24 h at: **(A)** 23 January 2012 09:00
9 LT, **(B)** 31 January 2012 21:00 LT, **(C)** 6 February 2012 18:00 LT; particle
10 concentrations increase from blue to red.
11